Innovative Exploration Techniques for Geothermal Assessment at Jemez Pueblo, New Mexico

Final Report DOE DE-EE0002841

June 28, 2015

Author: Michael Albrecht

Contributors: Dr. Shari Kelley
Dr. Fraser Goff
Dr. Jamie Gardner
Dr. Giday WoldeGabriel
Virgil Welch

Acknowledgements

In addition to the contributors to this report we acknowledge the contributions and support of the following participants in the project:

All Governors of the Pueblo of Jemez

All members of the Pueblo of Jemez Finance Department

All members of the Pueblo of Jemez Human Resource Department

All members of the Pueblo of Jemez Transportation Department

All members of the Pueblo of Jemez Natural Resources Department (NRD)

Greg Kaufman, NRD Director and Project Manager 2010 to 2014

John Galvan, Interim NRD Director

Dr. William Inskeep, Hydrogeochemistry Consultant

Robert “Zeke” Salaz, Graduate Student NM Tech

All members of the PASSCAL Instrument Center, NM Tech

Dr. Lianjie Huang, LANL Scientist

Kenneth Rehfeldt, LANL Team Leader

Virgil Welch, Drilling Manager

All members of TBA Power’s “Team Wolverine”

All subcontractors of TBA Power

and countless others.

Table of Contents

calculated from analyses of natural waters in the Jemez Pueblo region, New Mexico
(b) Fraser, G., 2010, Preliminary Notes on Jemez Pueblo Region Isotope Data

Appendix C:
(a) Zonge International Inc., 2011, Geophysical Investigation Report, 2D Seismic Reflection Survey Jemez Geothermal Project
(b) Seismic Source sample data.

Appendix D:
Dewhurst Group, 2011, Final Report: Magnetotelluric Survey Pueblo of Jemez, New Mexico

Appendix E:
Selman and Associates, 2013, Mud Log Jemez-GT-01, Pueblo of Jemez, New Mexico

1. Results of the Exploration Surveys

1.1 Geology and Mineralogy

The Indian Springs thermal area lies on the banks of the Jemez River 3.5 km southwest of the village of Jemez Pueblo. The springs are located in the southwestern Jemez Mountains in north central New Mexico. A detailed geologic map of ~eight square miles of the south-central Jemez Reservation in the Indian Springs area was produced at a scale of 1:10,000. Regional scale geologic maps of the Jemez Mountains include the maps of Wood and Northrop (1946), Smith et al. (1970), Kelley (1977), and Woodward (1987). The Quaternary terrace and pediment deposits shown on the geologic map of the Indian Springs area were modified from published 1:24,000 geologic maps of the San Ysidro quadrangle (Woodward and Ruetschilling, 1976; Formento-Trigilio and Pazzaglia, 1998) and the Jemez Pueblo quadrangle (Pazzaglia et al., 1998). Faults and other distinctive features, such as iron mineralization and travertine deposits, that might indicate the presence of geothermal water in the recent geologic past were highlighted and analyzed in detail. Although the conducted work describes the bedrock geology both west and east of the floodplain of the Jemez River, most of the effort in this investigation was focused on the faulted area to the west of the Jemez River. The occurrences of three generations of travertine deposits within the Pueblo of Jemez along the Jemez fault zone suggest that these rocks are contemporaneous and related to the same hydrothermal system that originated beneath the Valles Caldera (Goff and Shevenell, 1987; Goff et al., 1988). The mineralogical compositions of various samples were determined by powder X-ray diffraction. With regard to some secondary illite, kaolinite, Fe-oxides and quartz contents of altered Quaternary pediment gravels, it is not clear whether all alteration took place in situ or if some gravel was partially altered before transport to its current location. If the alteration took place in situ, it is possible that the gravel was affected by high-temperature (>100ºC) hydrothermal activity.

In summary, the sequence of Quaternary hydrothermal events as recorded in the study area through U-series dating at Travertine Hill, Bluewater Canyon, and Salt Spring includes:

- Deposition of a fine-grained, laminated, clay-bearing silty lake deposit with interbedded organic material across the Jemez fault zone. This lacustrine deposit contains illite, but it is not clear if the illite is detrital or if the clay grew *in situ*.
- Deposition of the oldest travertine at ca. 233 ka.
- Deposition of the Qp4 pediment.
- Hematite accumulation within the Triassic Shinarump Formation near Travertine Hill. The Qp4 pediment, and Shinarump and Zia formations in Bluewater Canyon were likely mineralized at the same time, although the stratigraphic relations are less clear to the north. Illite formation accompanied hematite mineralization, suggesting temperatures >100°C.
- Deposition of the middle travertine on top of the hematite-altered Shinarump Formation near Travertine Hill. The middle travertine gave a ca. 144 ka U-series age, but the errors are so large, so the age is considered suspect.
- Accumulation of travertine along a NW-striking vent at ca. 166 ka near Salt Spring. This vent may have fed higher elevation travertine deposits north of Salt Spring. The vent appears to have been exhumed and is now surrounded by 50 ka Qt5 alluvium.

Supporting documents and more details can be found in the updated subject matter report by Dr. Giday Woldegabriel & Dr. Shari Kelley from April 2011, entitled “Mineralogy, Petrography, Geochemistry, and

U-Series Dating of Travertine and Sedimentary Rocks from Pueblo of Jemez, New Mexico", Appendix A. That report was funded by this project and is not the result of a separate LANL study.

1.2 Hydrogeochemistry

A very comprehensive water sampling protocol has been conducted in the study area, sampling at 14 locations and utilizing 31 years of historical data in the region (see Appendix B, Goff 2010 a and b). Major and trace element chemistry and stable isotope analyses on the 14 new samples as well as a variety of geothermometry calculations on the combined data sets have been performed. As a result of this hydrogeochemical investigation, it is very certain that the fluids observed in the Indian Springs well are of shallow origin including the Valles Caldera outflow plume at a depth of about 240 ft and a temperature of about 68 ºC. Similarly, mixing with deeper resource fluids does not appear to be taking place in other analyzed springs as well.

In order to better understand the origin of the fluids that enter Jemez-GT-01 (see Figure 16) in Mississippian, two fluid samples from the well have been analyzed. The first an "air lift" sample collected in early November and the second a flowing sample collected early December 2013. The collection temperatures of both samples were <50 °C. The chemistry data show that the Jemez -GT-01 waters are reasonably close in general chemistry to the waters of Salt Spring and the Indian Springs (JP-1) well. This is somewhat expected, especially for the first sample, because JP-1 water was used as water source for the drilling operation of Jemez-GT-01. The most noteworthy differences in the two samples are 1) a slight decrease in the concentrations of some key constituents (Na, K, Li, F, Cl, Br, SO4, B and As), 2) a pronounced increase in SiO2, and 3) slight increases in the divalent cations (Ca, Mg and Sr). From these differences, it appears that the down hole composition of uncontaminated Jemez-GT-01 water is slightly less concentrated than JP-1, has a slightly higher equilibration temperature (hence higher SiO2), and is mixed with a different source of divalent cations.

Following an average analysis of Soda Dam (main) water based on 10 samples collected between 1991 and 2004, Soda Dam water originates by mixing of hot geothermal brine from the 260-300 °C Valles caldera geothermal system with cool Ca,Mg,Sr bicarbonate waters along a hydrothermal outflow plume extending southwest of the caldera. Superficially, there are similarities between the waters collected at Jemez-GT-01, Salt Spring, JP-1 waters and Soda Dam water. Key differences: 1) Soda Dam water contains significantly more K relative to Na than the other waters and 2) Soda Dam water contains more Li, Br, B, As (and probably Cs and Rb) relative to Cl than the other waters. Also, there are important differences in the comparative amounts of F and SO4. Those differences can be interpreted to mean that the geothermal component of Soda Dam water (very high K) equilibrated at much higher temperature than the waters collected at Jemez-GT-01 and its nearby relatives.

The best indications of temperature for the fluids collected at Jemez-GT-01 come from silica geothermometers and cation geothermometers that account for Mg (and other low-T components). Silica geothermometers also provide a good indicator of temperature in moderate- to low-temperature samples. The samples from Jemez-GT-01 are most likely equilibrated at somewhere between 110 and 70 °C. The flowing sample is probably most representative of downhole conditions. Further logging and hydrogeological well testing are needed to better describe the waters known to be present and those possibly sampled in future at the bottom of the well.

1.3 Seismic

To obtain high-resolution images of subsurface geologic structures of the potential target geothermal reservoir at the Pueblo of Jemez, active seismic reflection surveys were conducted along three lines using a static array at 50ft source-receiver spacing in order to accommodate pre-stack depth migration specifications (see Figure 1) and an accelerated weight-drop seismic source (see Figure 2). A detailed discussion of the seismic studies is included as Appendix C (a) (Zonge International, Inc, 2011).

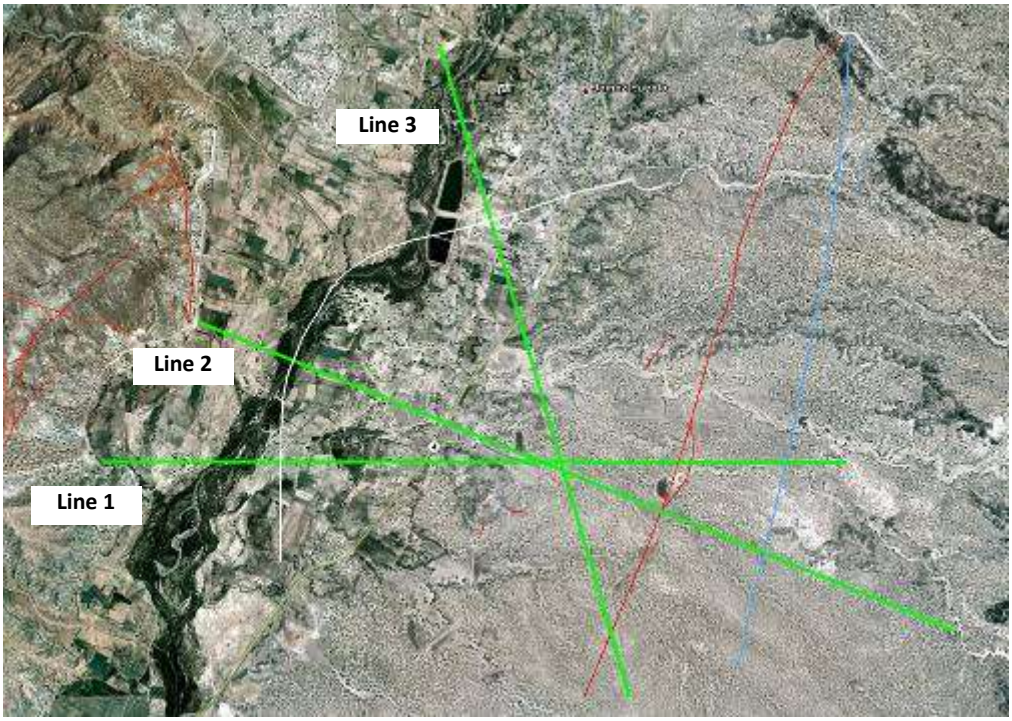

Figure 1: 2-D seismic reflection survey lines conducted in the study area. According to previous geologic studies of the fault system in the area by Witcher (2004) the white curved line represents the Indian Springs Fault Zone, and the light blue line in the east represents the Vallecito Creek Fault Zone. The red lines to the west are the result of Phase 1 mapping related to the Jemez Fault Zone. The red lines in the east are the result of Phase 1 mapping of the Vallecito Creek Fault Zone.

The seismic source chosen (see Figure 2) can reach in excess of 8,000 feet to 10,000 feet. Sample data used during the source selection process (see Appendix C (b)) reach as deep as 21,000 feet. The source is not a vibroseis but a high impact source powered by compressed nitrogen. The 1450 lbs hammer generates over 500,000 ft/lbs of energy per shot. The data presented to aid in the source selection show that the high impact source yields better data quality than dynamite and vibroseis.

The information used to support and calibrate the seismic interpretation are limited to surface geological maps, geological cross sections, regional well log data and written reports. Wells to the northwest of the

study area were used to get a range of possible velocities for the Jurassic and older rocks and for the shallow sediments. No project area well data were sufficient to aid in the interpretations.

The fault offsets seen on these seismic interpretations are dependent on the seismic events (or horizons) that were picked on either side of a fault. The reason that the flattened seismic sections (see Appendix C (a), Figures 15 to 17) were shown in the seismic report was to establish the certainty of the event correlations across each fault. The red unconformity event was selected as the flattened event. These displays clearly establish the lateral correlations of seismic events and shows the existing structure of the area at the time of this erosional surface. Rift faulting has subsequently offset these seismic events (the pre-existing structure/stratigraphy) to give us today's structures.

Figure 2: An AXIS accelerated weight-drop seismic source with 500,000 ft/lbs of energy per shot was used for the seismic surveys.

The Indian Springs main fault has the largest vertical displacement and is readily seen on lines L1 and L2. With that amount of vertical offset, it would be readily apparent if it crossed line L3. It clearly does not cross that line and has been interpreted to miss the northwest end of that line (see seismic structure maps, Appendix C (a), Figure 19 to 27). Witcher (2004) has shown another fault in that position (off the end of L3) and that fault is probably the northern extension of the Indian Springs main fault. There is no evidence for a south to southeastern dipping line crossing the northern half of line L3. Therefore, the Witcher (2004) mapping of an eastwards bend in the Indian Springs fault zone either does not occur or the fault does not reach L3. Other small faults are observed on the northern half of L3, but they have the opposite dip (i.e. north dip), which is inconsistent with the Indian Springs fault geometry.

All average velocity corrected, time migrated seismic lines are displayed in Figure 3 (a) to (c).

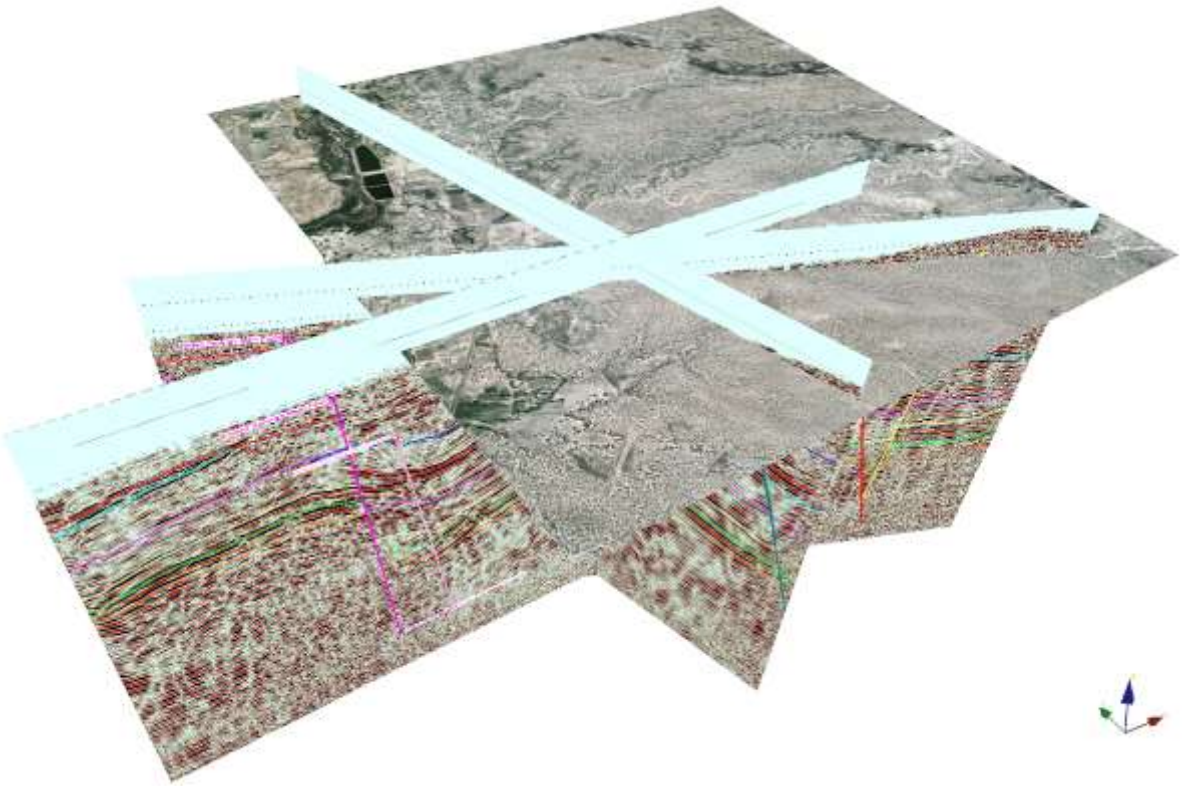

(a) View from the southwest of the study area

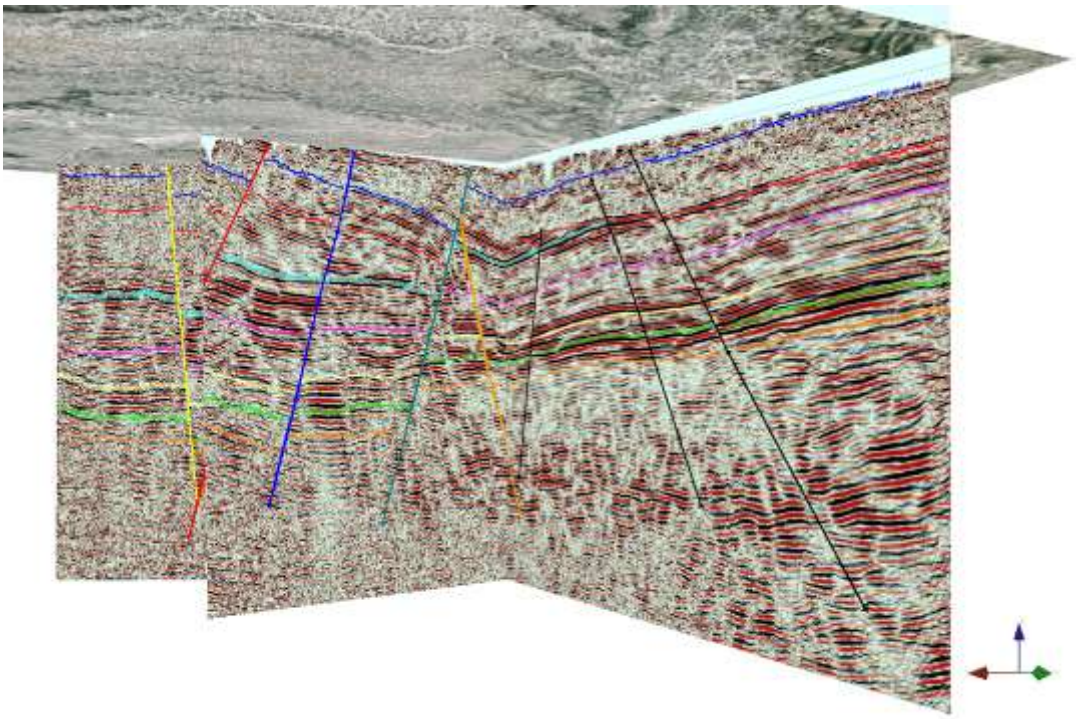

(b) View from the northwest of the study area from below the surface

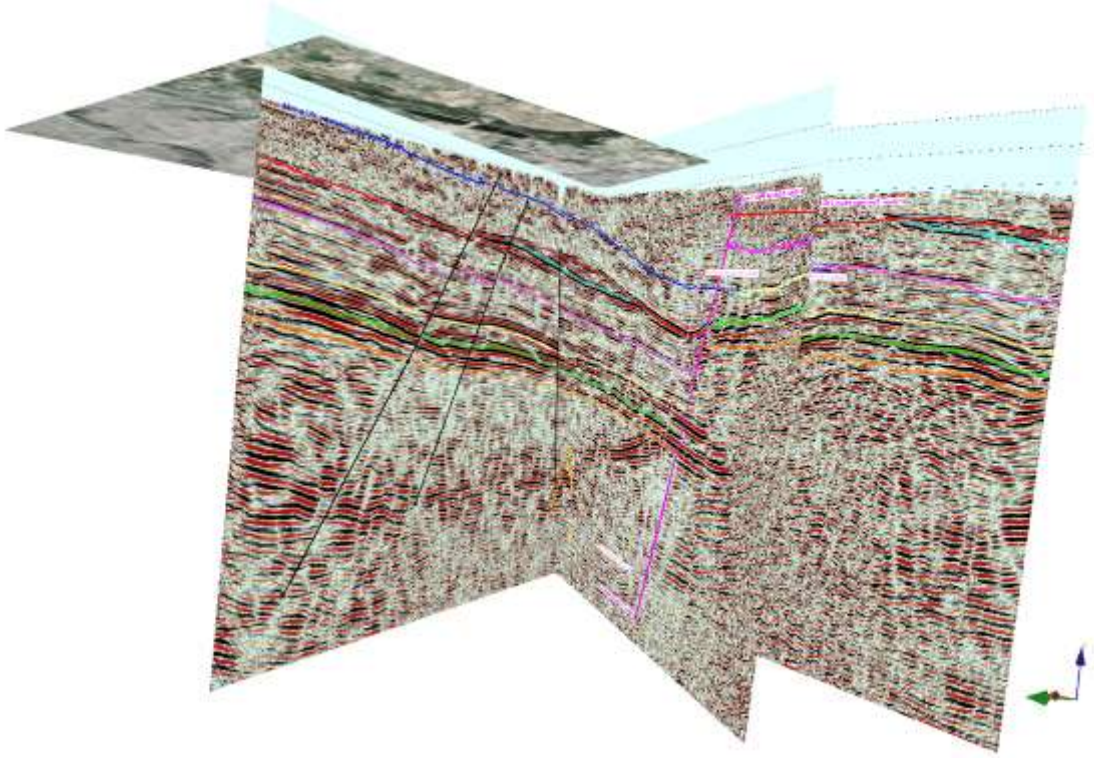

(c) View from the northwest of the study area below the surface

Figure 3: 3-D visualization of the interpreted seismic conducted in the geothermal study area.

Figure 4 (a) to (c) show the interpreted seismic profiles. The red line marked Unc might be an unconformity between Tertiary basin fill sediments (Santa Fe Group, etc.) above and Mesozoic-Paleozoic strata below. The orange line probably marks the boundary between the Paleozoic above and Precambrian rocks below. The rocks between the orange, green and yellow lines are likely Mississippian to Pennsylvanian limestones, sandstones and shales. The rocks between the yellow and magenta lines might be the Permian Abo Formation. The rocks between the magenta and light blue lines might be the Permian Yeso Group, Permian Glorieta Sandstone, Triassic Moenkopi Formation, and Triassic Shinarump (Agua Sarca) Sandstone. The rocks below the blue line and above the red unconformity line likely belong to the Petrified Forest Formation of the Chinle Group. The rocks above the unconformity could be syn-Laramide sediments like the Galisteo Formation. Rift fill sediments, including the Oligocene Gilman Conglomerate, the Oligocene-early Miocene Abiquiu Formation, and Miocene Zia Formation, might form the upper part of the section.

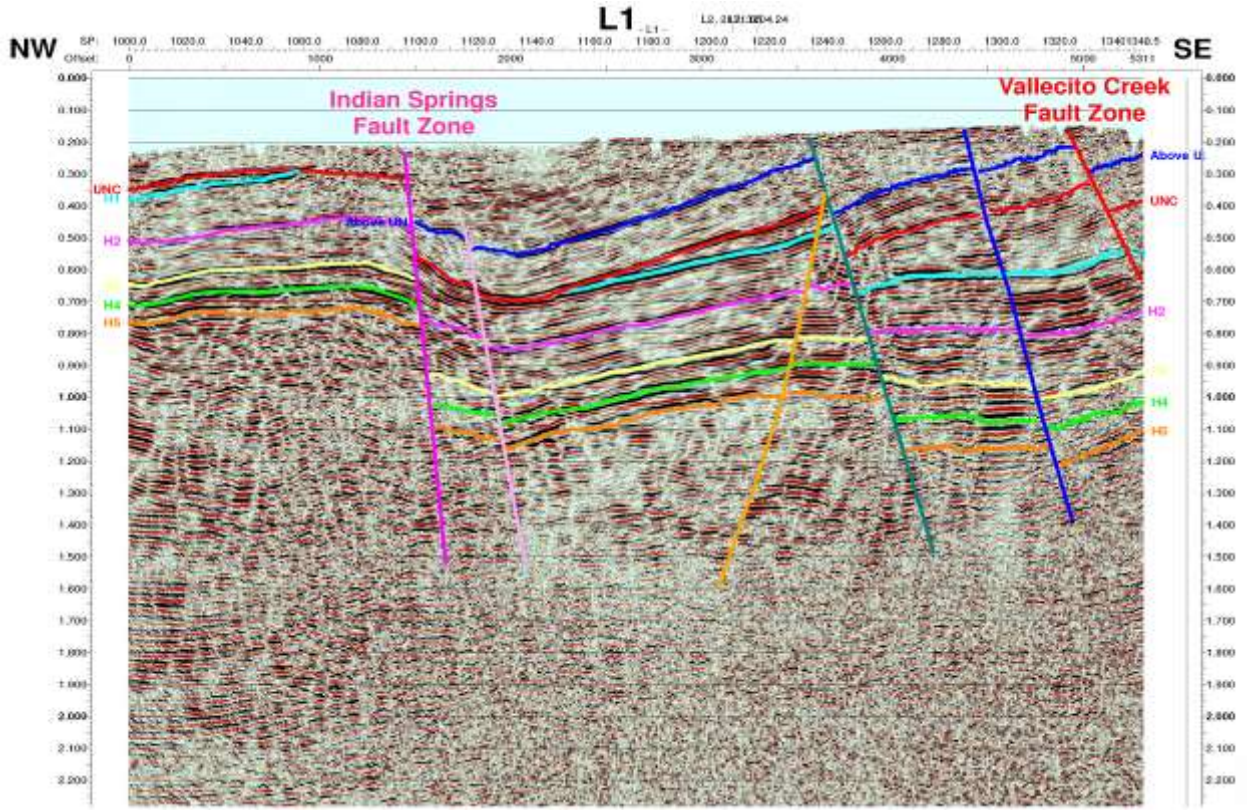

(a) Interpreted seismic line L1

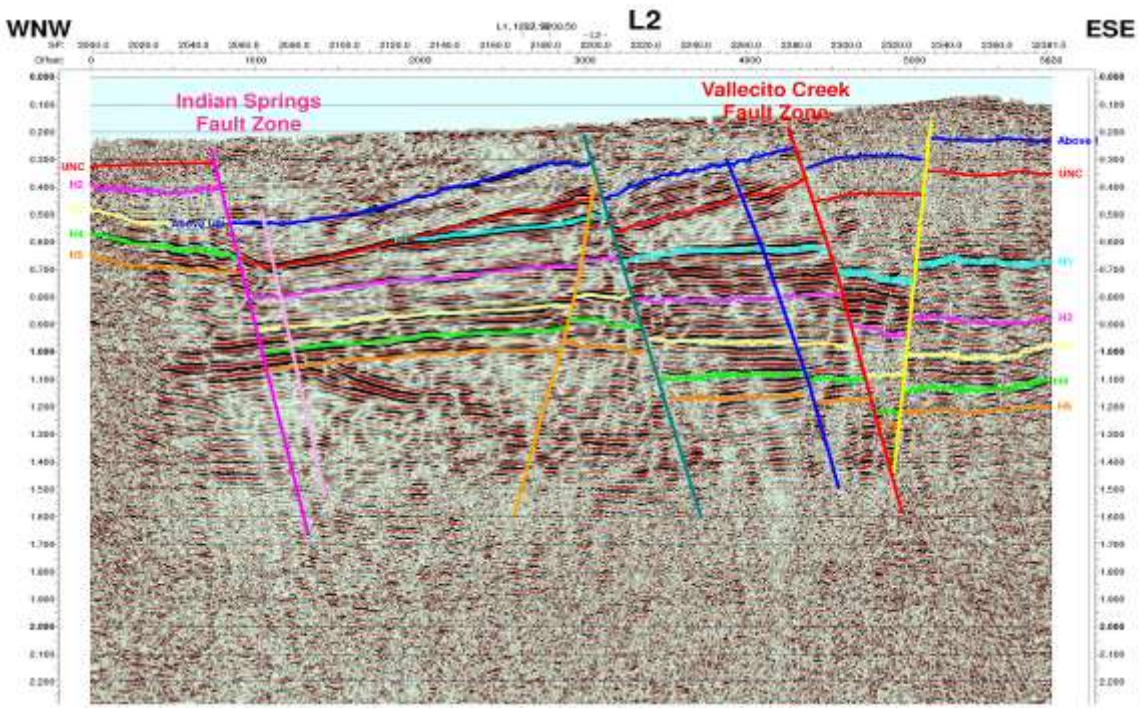

(b) Interpreted seismic line L2

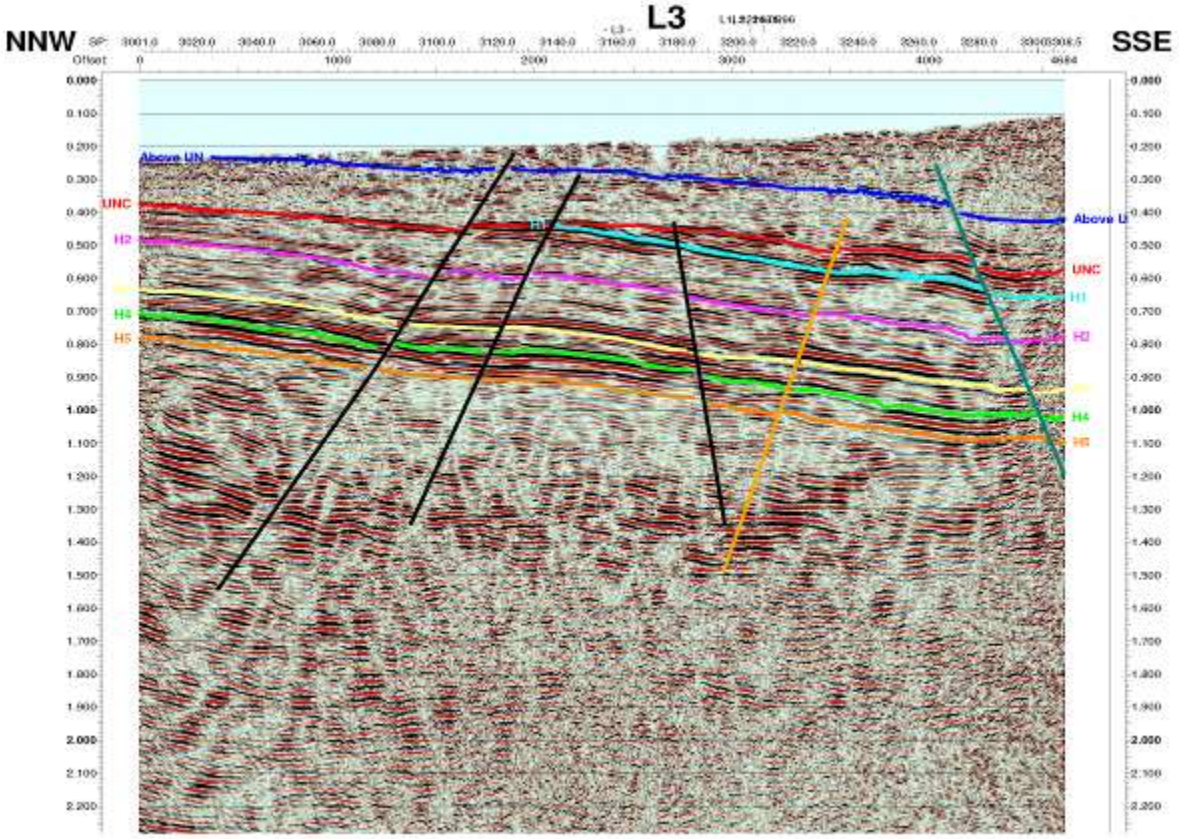

(c) Interpreted seismic line L3

Figure 4: Interpreted seismic lines

Importantly, seismic lines L1 and L2 identify a west-dipping half graben structure between the Indian Springs Fault Zone (west) and the Vallecito Creek Fault Zone (east). In particular, the interpreted orange fault trace has down-to-the-west displacement and no surface expression. This is unexpected. If correct, the graben may act as a trap for conductive thermal fluids. The second interesting thing is that the beds in this graben have an apparent structural rotation causing a pronounced dip to the west and the south. This may act like a structural trap for conductive fluids against the Indian Springs fault. The Indian Springs fault might have a Laramide history and may have started as a reverse fault dipping steeply west. That might explain some of the folding and complex structure in the fault zone.

For the development of the conceptual model as shown in Chapter 2, the seismic data have been depth migrated by a contractor of Zonge Inc.; in the course of the PreSDM Velocity Analysis and Imaging of the Jemez Pueblo 2D lines, prestack depth migration was run using both a Wave Equation algorithm (double downward continuation of shots and receivers with an imaging condition of zero downward continued offset and zero downward continued time) and a Kirchhoff algorithm. The two algorithmic results were very similar, but the Kirchhoff results were delivered.

Detailed models of both the interval velocity and the intrinsic layer anisotropy (η) were derived. In the PreSDM velocity analysis and imaging, the moveout correction for the intrinsic layer anisotropy was pre-applied to the input data, allowing direct PreSDM improvement of just the interval velocity.

The Kirchhoff PreSDM algorithm can be run directly from elevation, or equivalently, the input data can be upward continued using the wave equation to the desired flat datum, and then the Kirchhoff PreSDM algorithm may be run from the flat datum. In this case, the second option was utilized.

The Data Modeling Kirchhoff PreSDM uses a modified Runge-Kutta approach to solve the eikonal equation and calculate travel times from shot and receivers on the surface to all depth locations. These travel times are then used to combine all possible contributions to an output depth location. The eikonal travel time solver features handling of abrupt velocity contrasts and critical angle events, allowing the detailed, structurally consistent interval velocity to be adequately honored.

The input data to the Kirchhoff PreSDM is regularized prior to input, and is sorted into original common offset panels. PreSDM imaging is done for each common offset panel, producing PreSDM common offset gathers for inspection and velocity updating.

Lianjie Huang performed an innovative elastic-wave reverse-time migration with a wave field-separation imaging condition on the data (Huang et al. 2011). During that process the seismic section is "illuminated" from different angles. Figure 5 (a) and (b) shows the "illumination" process.

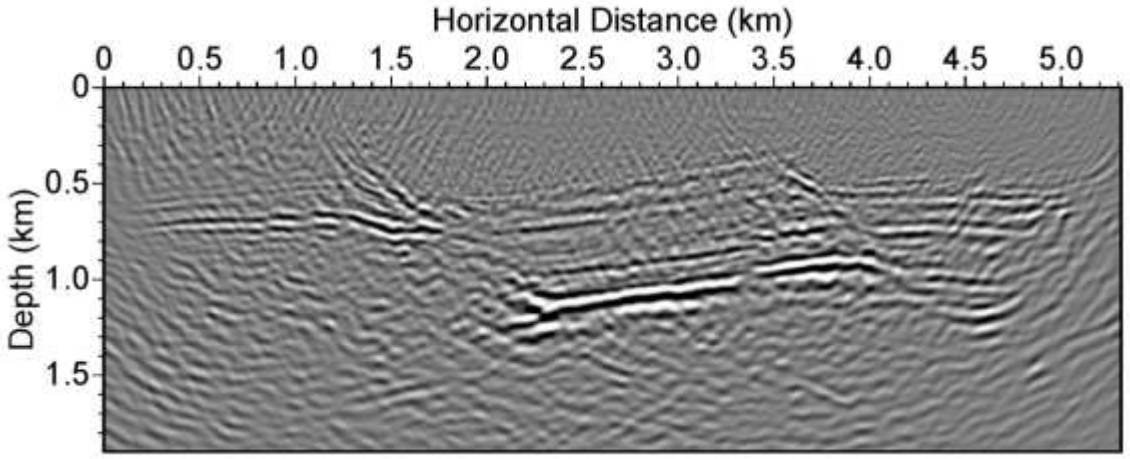

Figure 5 (a): Downward-looking image obtained using reverse-time migration of seismic data along Line 1.

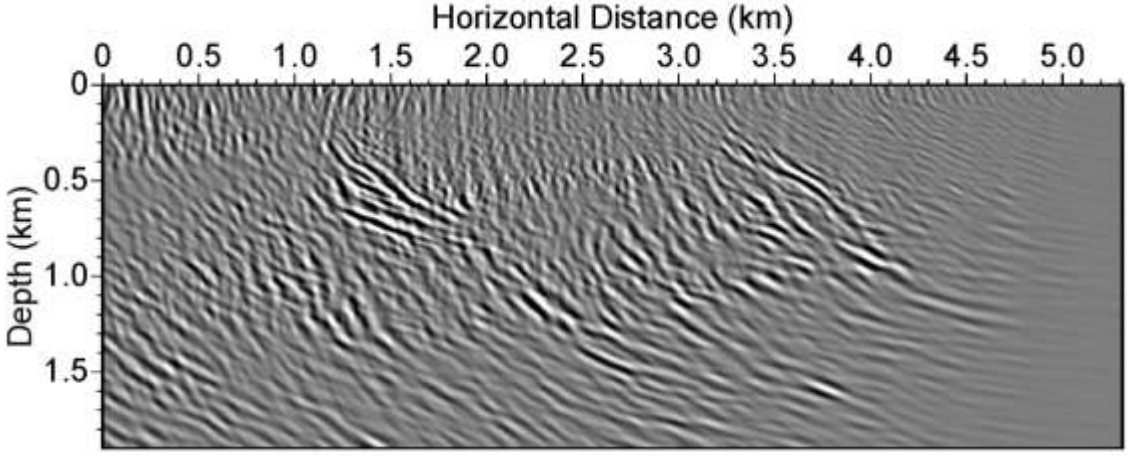

Figure 5 (b): Left-looking image obtained using reverse-time migration of seismic data along Line 1.

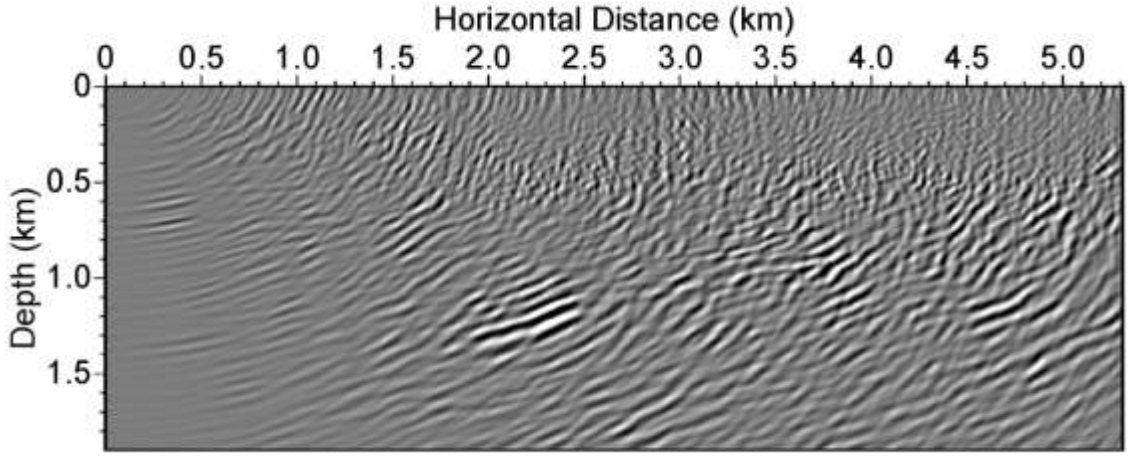

Figure 5 (c): Right-looking image obtained using reverse-time migration of seismic data along Line 1.

The geologic interpretation of the “illuminated” migration images as performed by Shari Kelley is depicted in Figure 6 superimposed onto the downward-looking migration image. The green lines are from the downward-looking image, the cyan lines are features enhanced by the right-looking image, and the black lines are those revealed by the left-looking image. Some of these features are in the vicinity of the faults and could be fracture zones.

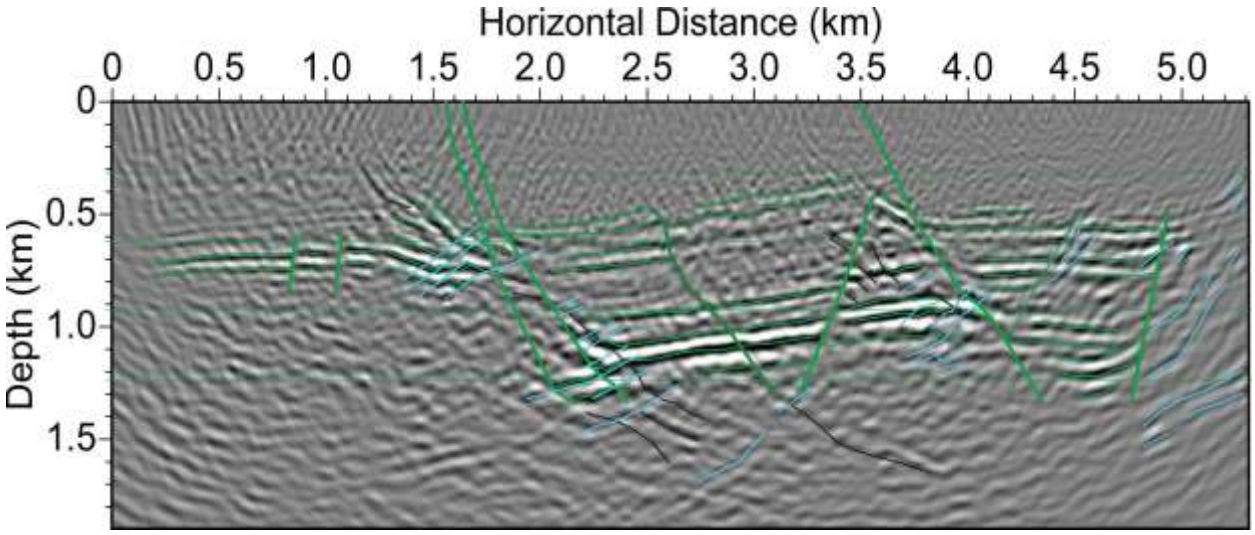

Figure 6: Faults revealed by the downward-, left- and right-looking images of reverse-time migration are superimposed onto the downward-looking image.

1.4 Magneto-Telluric

For magneto-telluric imaging 137 broadband MT (BMT) station observations have been conducted, resulting in 129 BMT 1-D inversions, 1 BMT 3-D rendering from 1-D data (1.5-D inversion), 13 BMT 2-D inversions (profiles), 1 BMT 3-D rendering from 2-D data (2.5-D inversion), and 6 unconstrained BMT 3-D inversions (see Appendix D). In addition to that 25 long-period MT (LMT) station observations with 24 LMT 1-D inversions and 14 LMT 2-D inversion profiles have been conducted. A total of 162 MT stations (both BMT and LMT) were used for observation (see Figure 7), and 153 of them were used for inversion. The receiver frequency range for LMT stations was 100 Hz to 0.0001 Hz and the frequency range for BMT was 1000 Hz to 0.001 Hz.

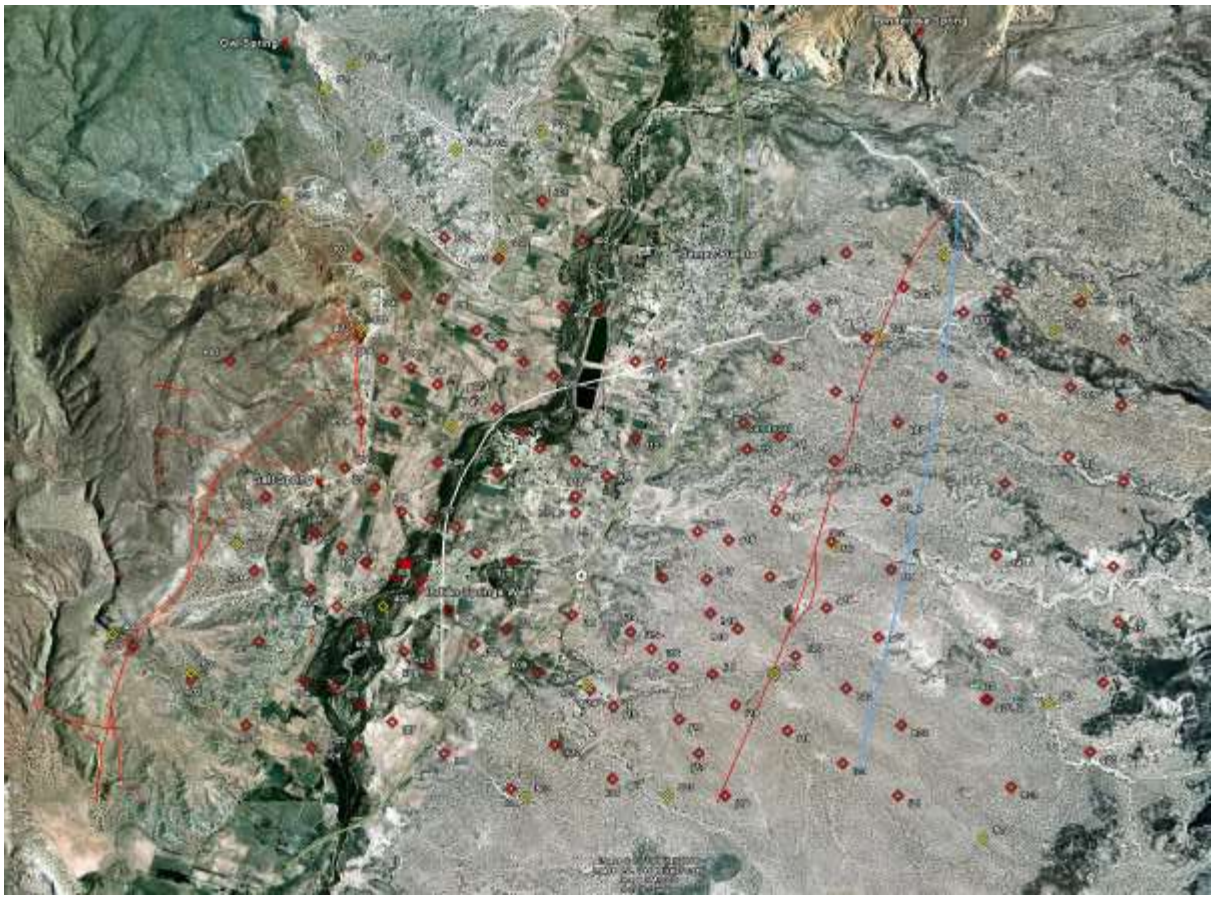

Figure 7: 137 BMT station observations and 25 LMT station observations conducted in the study area, covering the land east and west of Highway 4, south of the town center of Jemez Pueblo.

Following a detailed analysis of the distribution of electrical resistivity in the subsurface based on the processed inversions and in comparison with the seismic results, a favored high conductivity deeper

aquifer location or suitable entry point into a deeper aquifer has been identified. In the following this location is described as the “cup” (see Figure8 (a), (b) and Figure 9 (a) to (c)).

The rock resistivity depends on porosity and brine (salt water) content. The regions in red represent geologic formations with a resistivity of 10 Ohm-m or less. This is a good indicator for brine in the rock matrix of a geothermal reservoir or clays and geothermally altered “cap” rock. Such high conductivity at the “cup” would not exist if water would not be present and water would not be present to that extend if the rock wasn’t highly permeable and saturated.

Due to resolution limitations given the MT survey station spacing and the inversion depth, the depth of this highly permeable area along profile J might reach well beyond 1800 m. The steep blue and purple structures representing likely Precambrian basement or rocks with resistivity values which do not exclude igneous and volcanic rock, appear to be correlating well with the graben shown in the seismic results. The “cup” is a pronounced graben like structure just east of the Indian Springs Fault Zone that is probably a trap for high-conductivity fluids. Only drilling will show if the existing fluids are geothermal in nature or not.

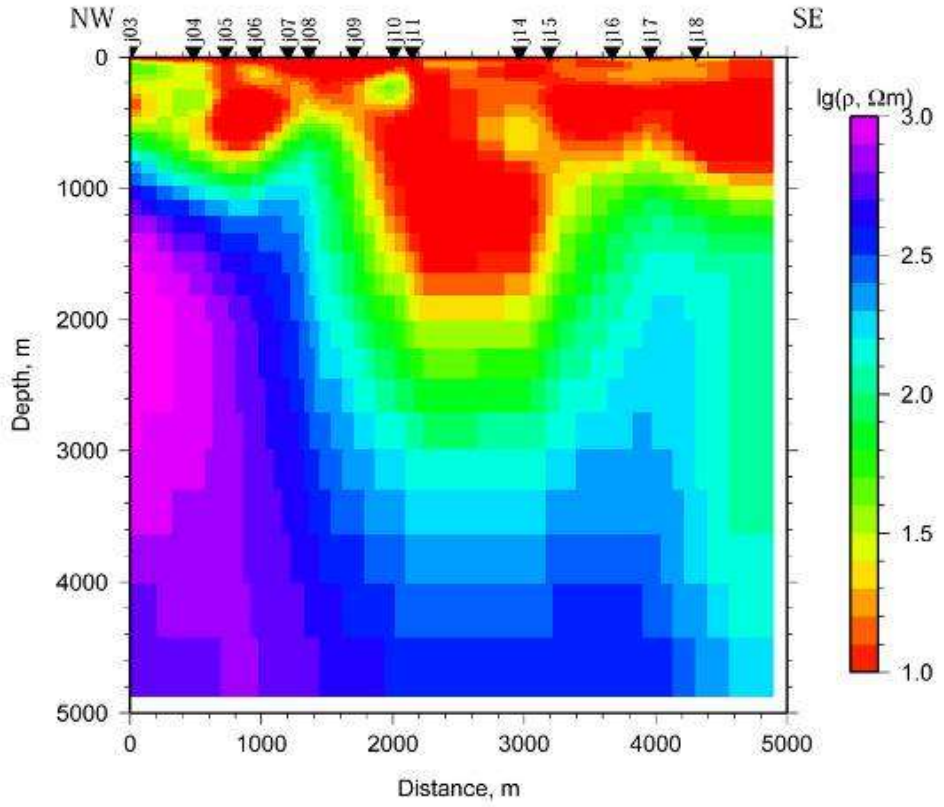

Figure 8 (a): 2-D inversion of BMT Profile J showing a highly conductive zone **reaching at least 1800 m deep** and confirming the steep and deep fault structures visible in seismic lines L1 and L2.

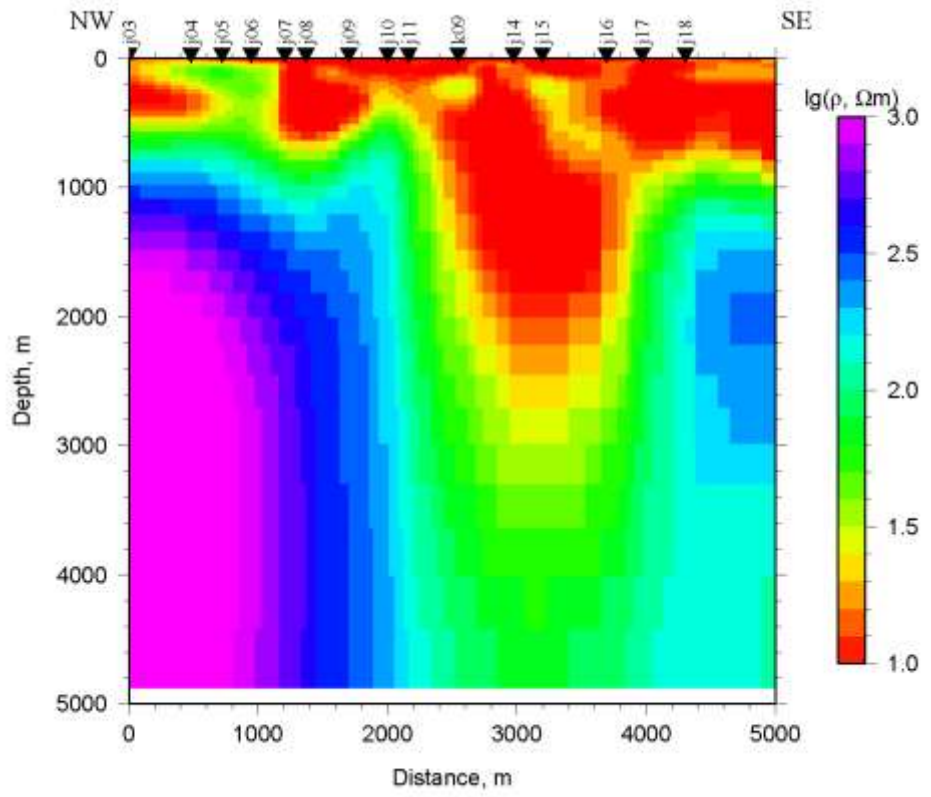

Figure 8 (b): 2-D inversion of BMT Profile J including station K09 showing a highly conductive zone **reaching deeper than 1800 m** and confirming the steep and deep fault structures visible in seismic lines L1 and L2.

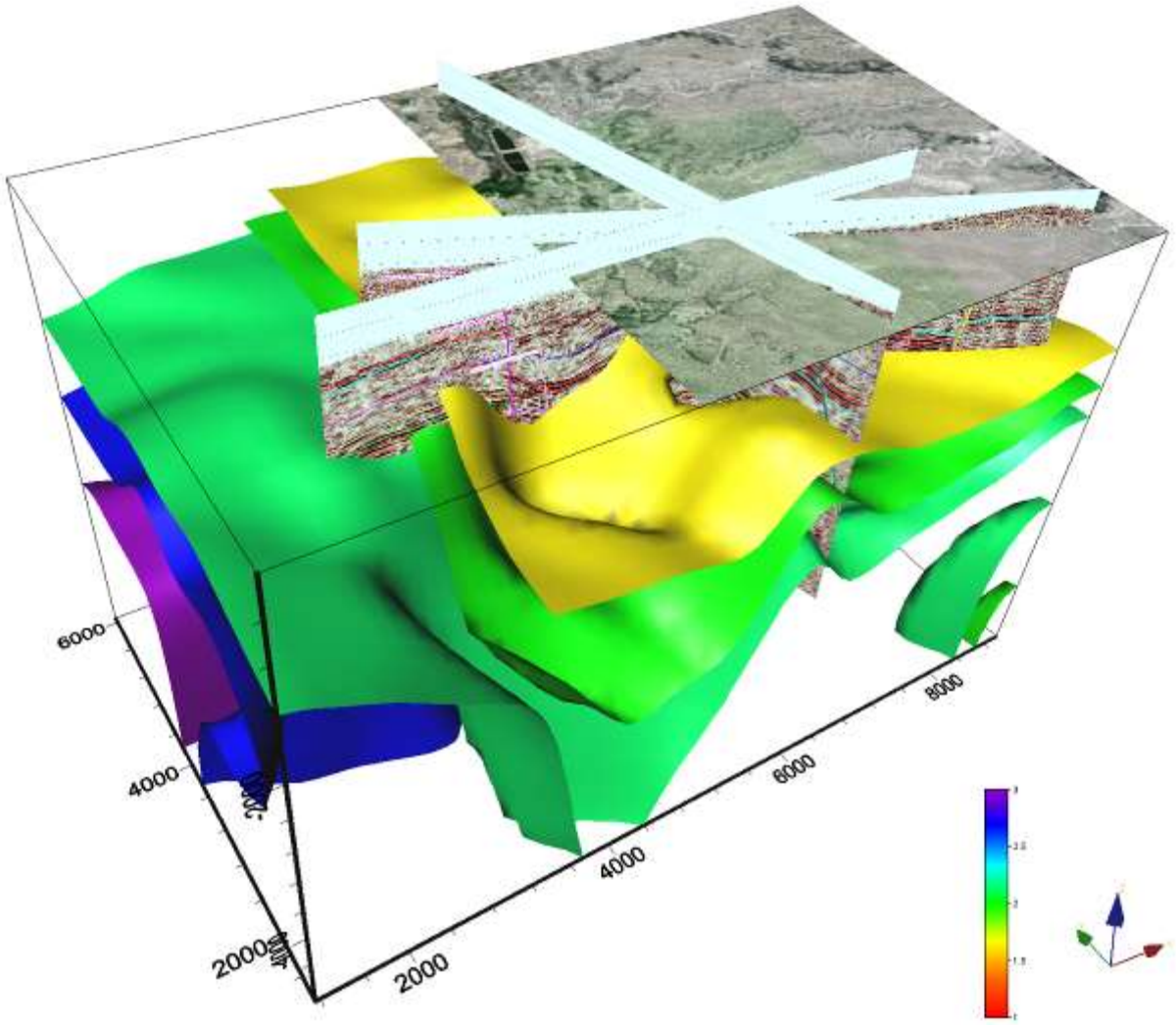

Figure 9 (a): 3-D integration of seismic and 2.5-D magneto-telluric data and the 2-D BMT Profile J. The “cup” defined by the 50 Ohm-m (yellow) and higher isosurfaces on a logarithmic resistivity scale.

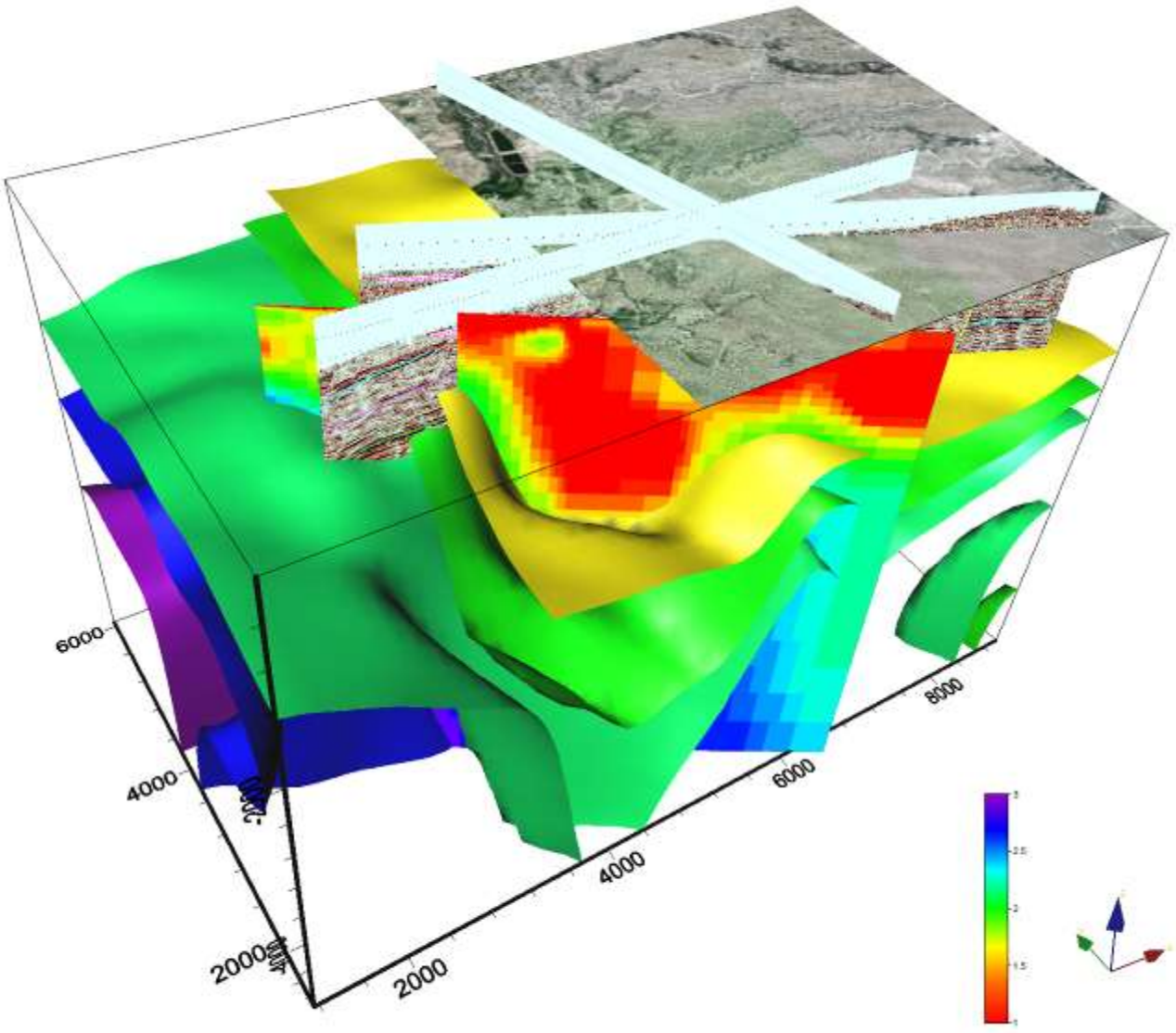

Figure 9 (b): 3-D integration of seismic and 2.5-D magneto-telluric data and the 2-D BMT Profile J. The "cup" as identified in the 2-D inversion of BMT Profile J.

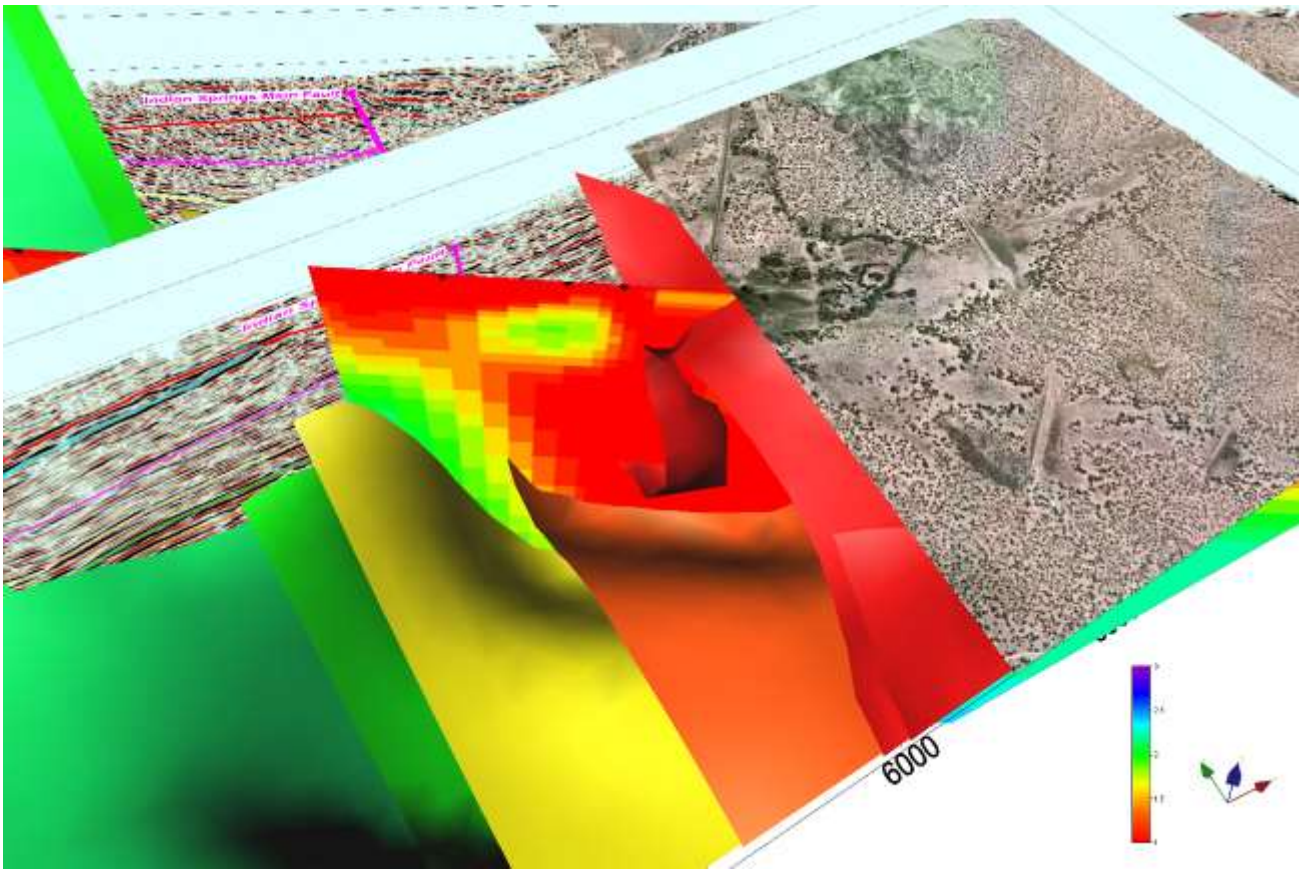

Figure 9 (c): 3-D integration of seismic and 2.5-D magneto-telluric data and the 2-D BMT Profile J. Close-up on the “cup”, focusing on the potential Drilling Target Area.

The 2-D Low Frequency Magneto-Telluric (LMT) inversions also indicate that a very deep heat source may be located below the Pueblo of Jemez (Figure 10).

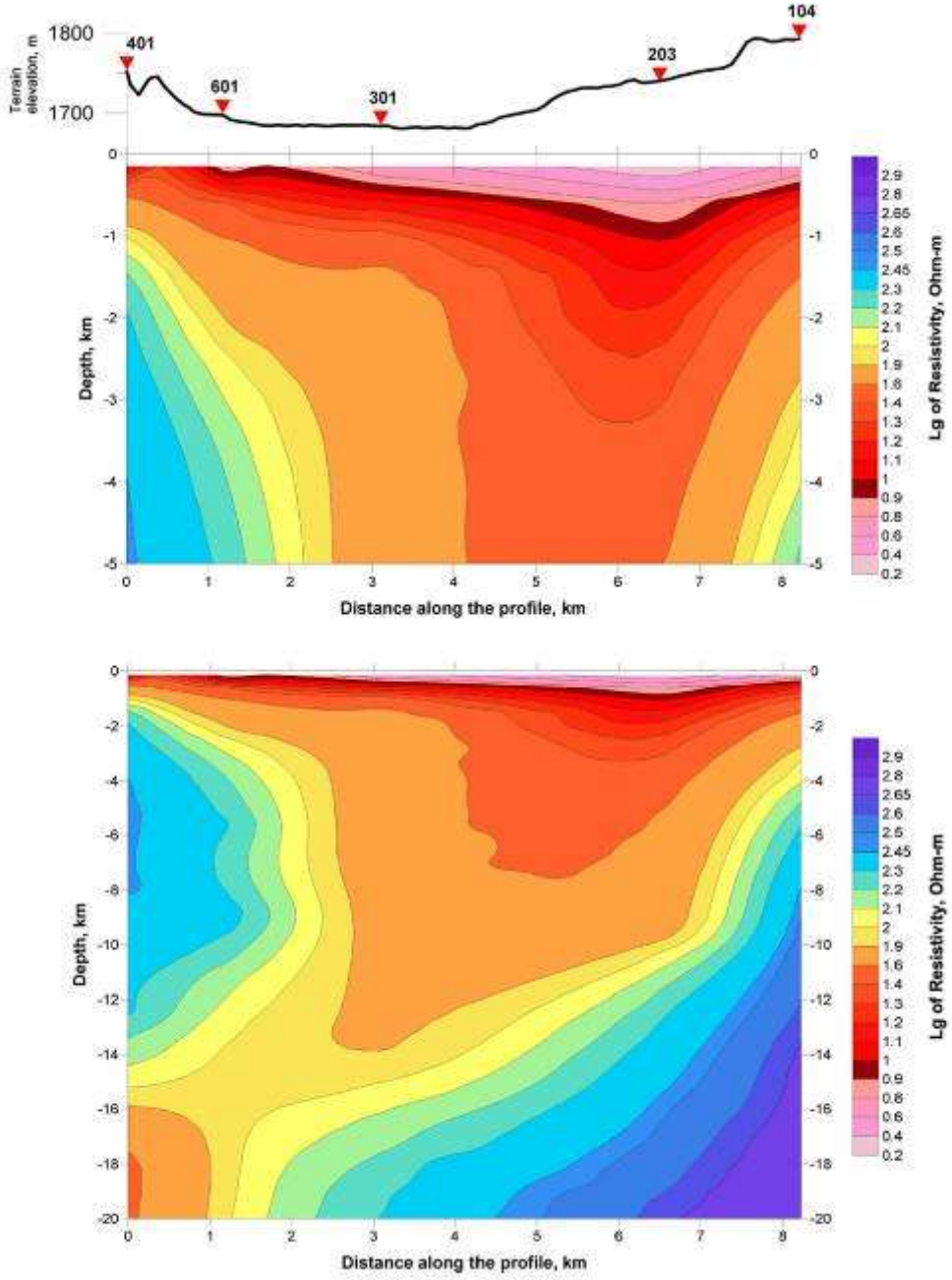

Figure 10: The LMT profile D indicates that the Pueblo of Jemez may be on the top of a deep heat anomaly. For more details see Appendix D.

Due to the lower frequency range observed during LMT surveys compared to the more commonly used Broadband Frequency Magneto-Telluric (BMT), the observation targets are located much deeper. Please note the difference in the depth scale between Figure 7 and Figure 5. In general more regional information

is obtained that might be of interest. In regards to the study area it appears to be interesting that a heat source of not more detailed characteristic appears to be located as deep as 20 km below the study area. Being located at the Valles caldera this does not appear too surprising.

When investigating the LMT data in more detail an area in the south-east corner of the study area has been found that is very interesting for geothermal power production. A large resistivity anomaly was detected along LMT profile L between stations 204, 405 and 504. Between station 405 and 504 the depth of the low resistivity values (1-1.4 Ohm-m) reaches more than 5,000 m. Comparing those results with the geological and tectonic settings it can be stated that the low resistivity zone is located in the Precambrian basement. This indicates that the south-east part of the study might host a huge fluid reservoir. Comparing the L profile with the profiles M, H, K and J indicates that the potential fluid reservoir is following a north-south orientation that leads out of the study area. Drilling for such a deep target would go well beyond the scope and budget of this project but it is something to consider for potential future commercial ventures even though the drilling depth would represent the deepest geothermal well in the United States.

2. Integrated Analysis

2.1 Conceptual Model

Figure 9 is an interpreted east-west cross-section that combines the results of geologic mapping with the seismic and magneto-telluric data. The stratigraphy is based on the true depth migrated seismic profile. The western third of the cross section across the Jemez fault zone is based on geologic mapping and the eastern two thirds is based on interpretation of Seismic Line 1. The rock units on the cross section were assigned using the relative reflectivity of units on the seismic lines and published thickness data. Thickness was measured upward from the Great Unconformity between the Proterozoic basement rocks and the Mississippian to Pennsylvanian sedimentary rocks. The lowest set of strong reflectors is interpreted to be Mississippian to Pennsylvanian carbonates. The seismically more transparent unit above the strong basal reflectors is likely the Abo Formation, which in this part of the Jemez Mountains is mainly siltstone with a few interbedded channel sandstones and conglomerates. The higher strong reflectors are interpreted to be Permian Yeso Group and Glorieta Sandstone, and Triassic Moenkopi Formation and overlying Shinarump Formation of the Chinle Group. Units above the pronounced unconformity on the Triassic rocks may include syn-Laramide Eocene Galisteo Formation (Tg), the Oligocene to Miocene Gilman Conglomerate and Abiquiu Formation (Tgc+Ta), and the Miocene Zia Formation (Tz).

The area outlined in yellow on the cross section shows the projection of the magneto-telluric anomaly located about 0.25 mile south of the section line onto Seismic Line 1, scaled appropriately. Jurassic units, most notably the Jurassic Todilto Formation, which contains gyspsum and limestone, are not present in this area, so the anomaly may be hot water rather than gypsum-saturated water. Magneto-telluric anomalies are not observed north along strike of the Indian Springs fault. Along south the survey boundaries are reached with potential inversion borderline limitations. The localized anomaly may be related to restricted, relatively recent, rupture along the fault.

Witcher (2004) had previously proposed that the warm water observed at Indian Spring and in JP-1 was localized as a consequence of juxtaposition of aquifers and aquitards, creating hydogeologic windows. Such a model would predict a relatively restricted stratigraphic range for the magneto-telluric anomaly. The fact that the anomaly cuts across stratigraphy suggests pervasive fracture porosity and permeability, assuming that the anomaly indicates hot water.

Past and present geothermal systems: Stratigraphic relations among travertines associated with the Jemez fault zone and other faults in the southwestern Jemez Mountains indicate multiple (at least four) episodes of travertine deposition. The travertine deposits place some constraints on the timing of high-temperature (>100°C), illite-forming hematite alteration near Travertine Hill. The Qp4 pediment conglomerate was deposited after 233 ka. Hematite alteration near Travertine Hill occurred prior to deposition of the middle travertine. The hematite alteration is poorly constrained to be older than 144 ka. Thus, this mineralization is relatively old.

The hydrogeochemical data gathered as part of this investigation with analyzed geothermometry and standard stable isotope data supports an outflow plume dominated system west of the Indian Springs Fault zone and indicates that the fluids observed in the Indian Springs well itself are of shallow origin; the shallow Valles caldera outflow plume is at a depth of about 240 ft and a temperature of about 68ºC.

Figure 11 and Figure 12 summarize the conceptual model for the resource, which builds on the model of Goff et al. (1988) and includes a shallow outflow plume and a deep convection system. The latter system, which is blind, holds the greatest possibility of commercial power production. The geologic cross-section runs down the Jemez River between Sulphur Springs and San Ysidro. The geology is reasonably well constrained by recent 1:24,000 scale geologic mapping (Goff et al., 2005; Kelley et al., 2003; Osburn et al., 2002; Pazzagila et al., 1998) and borehole data (VC1, VC2a, VC2b, JS1) north of Red Rocks. The isotherms are constrained by borehole data between the caldera and Jemez Springs (JS1). Older rock units along the river south of Red Rocks are buried by Quaternary floodplain deposits, but their depth and displacement can be loosely constrained, in part, by the interpreted seismic lines. The shallow outflow plume from the Valles caldera can be mapped as far south as JP1 on the Pueblo of Jemez (orange dashed line). Temperatures at depths greater than 254 ft south of JS1 in Jemez Springs are not known. The projected depth of the 100°C isotherm on the south end of the cross section is based on a few BHT data and one equilibrium temperature log from oil wells several kilometers west of San Ysidro on the Colorado Plateau. The red line shows the approximate position of the 100°C isotherm using the Jemez Springs and San Ysidro data as end points.

A speculative model of deep temperatures in the southwestern Jemez Mountains is depicted by the dashed red line (see Figure 12). This testable hypothesis is based on temperature-depth observations of Harrison et al. (1986) at Fenton Hill and Shevnell et al. (1988) in AET-4, which is located just northeast of Jemez Springs on the downthown side of the Jemez and Cat Mesa fault systems. T-D data from Fenton Hill show lateral flow of hot water at the Proterozoic-Late Paleozoic contact, T-D data from AET-4 shows lateral flow of 120°C water within the Madera Limestone, about 100 m above the basement contact. Although no lateral flow at the basement contact is observed at Jemez Springs Goff et al. (1988), it is possible that deep, south-directed lateral flow has stepped east of the Cat Mesa and Jemez fault systems and is now migrating south along the Vallecito and Jose fault systems.

Figure 13 shows the superposition of the reverse-time seismic migration results with the results of the other structural studies and standard seismic processing as performed in this project. That superposition has been used as a basis for the drilling planning.

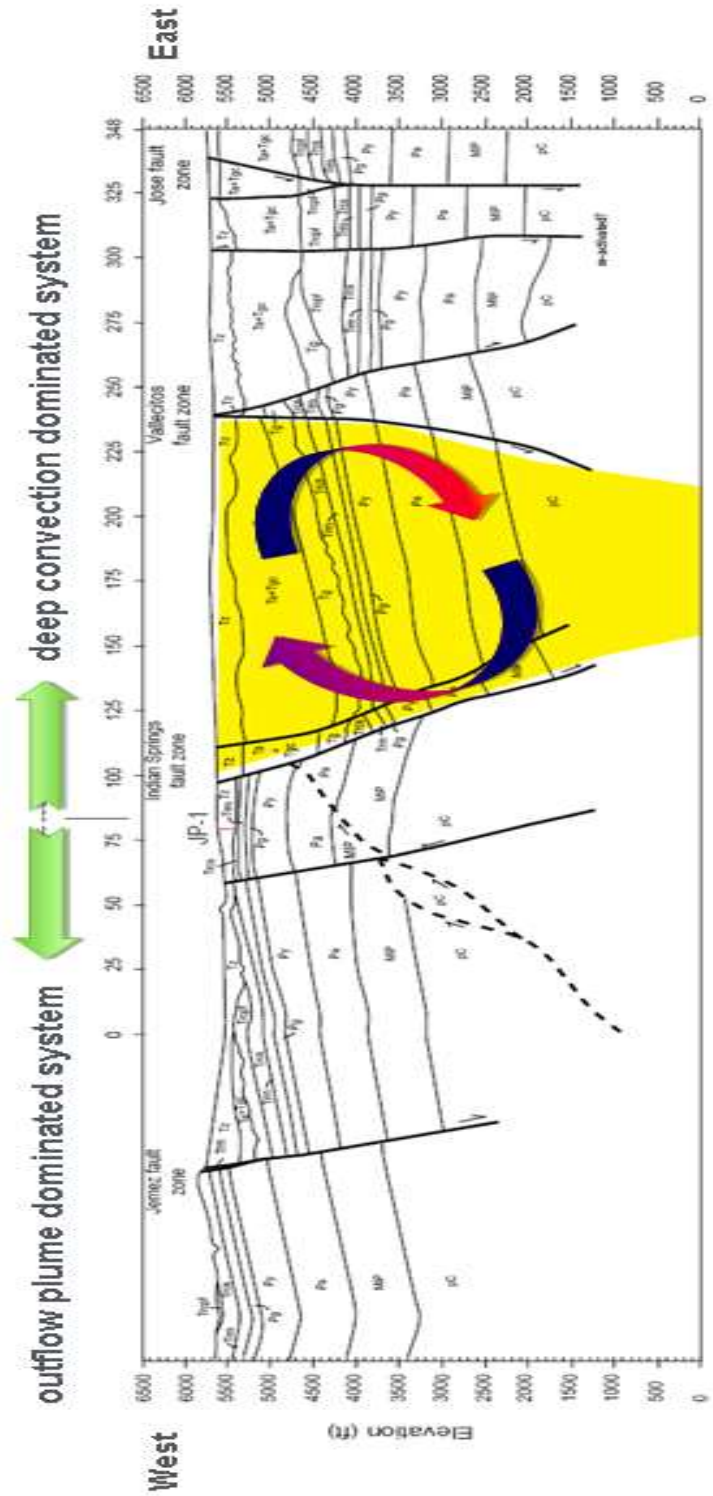

Figure 11: Geologic interpretation of seismic line 1. The yellow area is the zone that hosts the magneto-telluric anomaly. It is reasonable to assume that convection cell(s) are presented in that zone and have to be analyzed after the drilling through well logging and hydrogeological well testing.

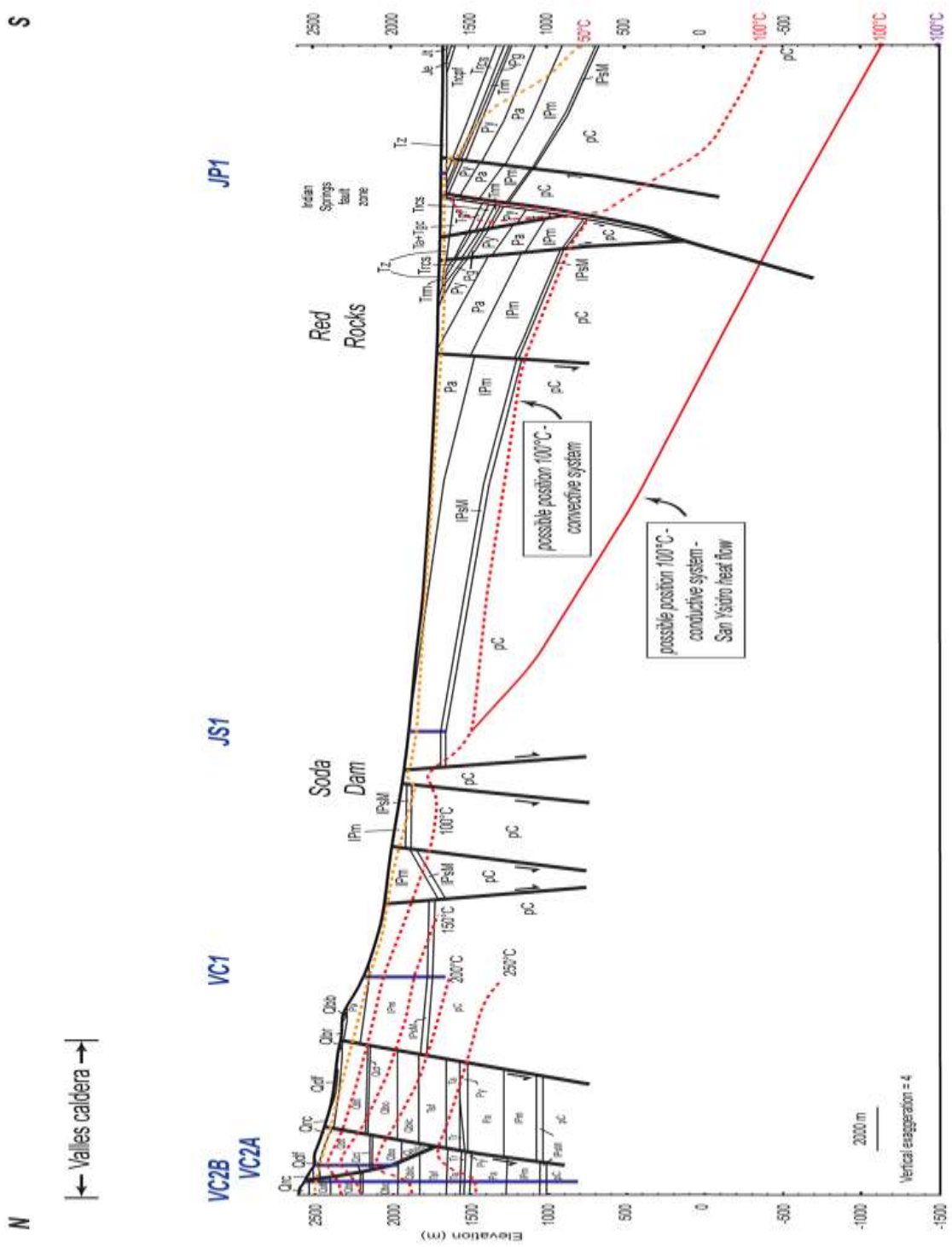

Figure 12: Conservative temperature isotherm modeling based upon BHT data in the Colorado Plateau and the upper Valles caldera system. Assessments have been made for a conductive (red line) and a convective system (red dotted line).

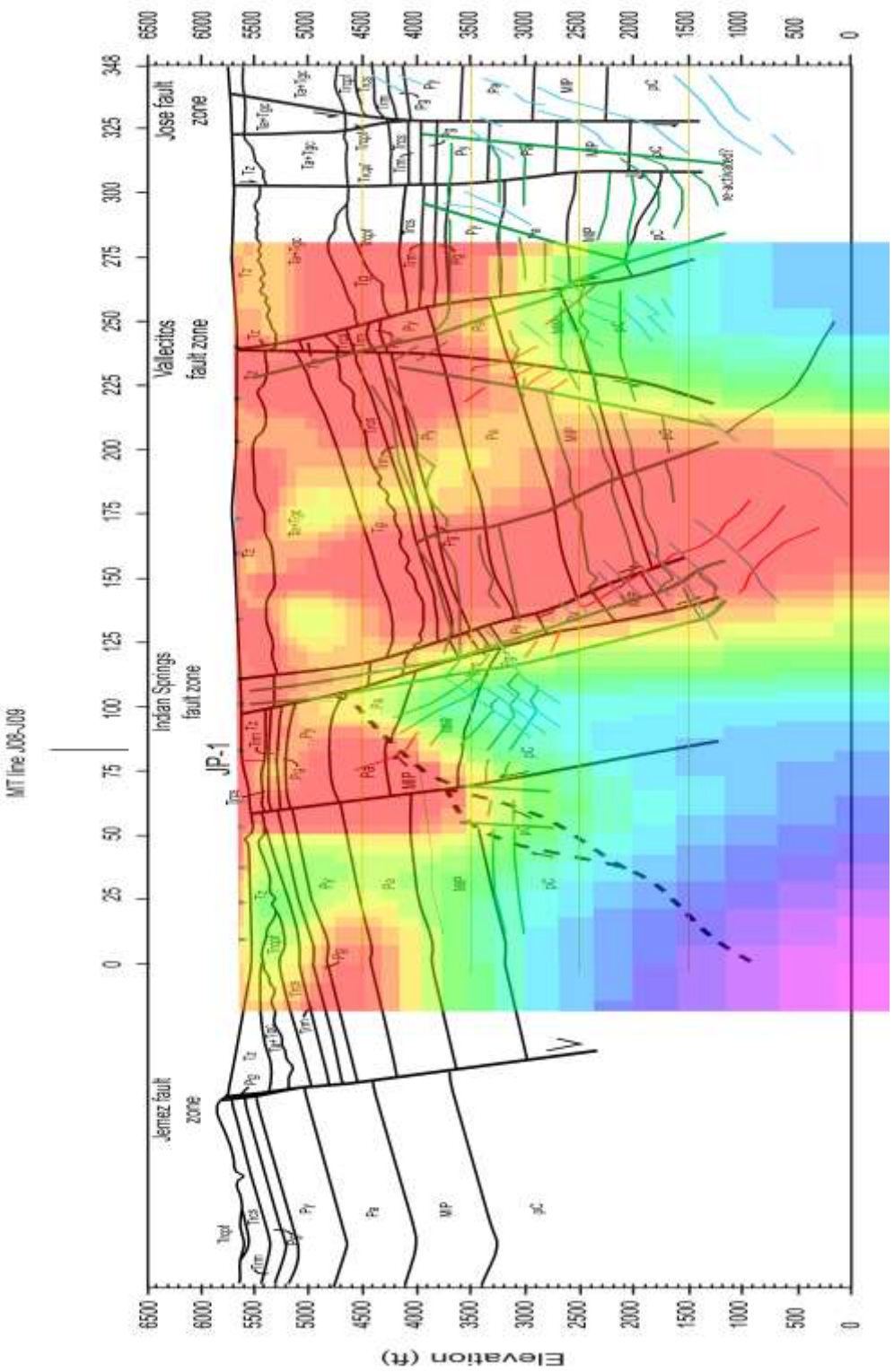

Figure 13: Superposition of BMT Profile J (see Figure 8 (b)), the reverse-time seismic migration results (green, blue and red) with the results of the other structural studies and the standard Kirchhoff seismic depth migration (black).

2.2 Inferred Resource

Following Williams et al. (2008) many geothermal reservoirs are dominated by fracture porosity, which can be characterized by high permeabilities but relatively low fluid volumes. Based on our geophysical surveys, the study area appears to be dominated not by simple vertical or horizontal conduits of limited spatial extent but by multiple vertical conduits grouped in fault zones to the west and to the east of a structural basin or "cup", showing heterogeneous permeability along the dominantly northeast to southwest trending structures throughout the complete study area. With two or more fault damage zones of 100 to 500 m width, the total horizontal permeability should be considerable.

The temperature of geothermal fluids relative to the background geothermal gradient defines the maximum depth of circulation. As described earlier, this aspect, the vertical extent of the reservoir needs to be defined through drilling. Our magneto-telluric studies show a well-defined potential fluid trap reaching about 1800 m deep, which is potentially connected to very permeable fault zones. Station spacing and depth limit the resolution of the MT survey; thus it may not resolve deeper penetrating, fault-localized, circulating fluids in reservoir(s) with lower fluid volumes but potentially (much) higher temperatures. Temperature estimates as referred to in Goff (2010, see Appendix B), do not apply for the targeted deep fluid trap as there is no reason to assume nor have been findings identified suggesting that those deeper fluids are structurally connected to any of the hot springs analyzed by Goff (2010). The same applies to the fluid flowing artesian after the drilling, as described in chapter 4.3. Due to the analysis of the artesian water, it is currently assumed that it originates from a surface recharge penetrating through the highly permeable Mississippian. Because the well is not cased in the permeable Mississippian, the pressure the fluid is under causes it to rise in the wellbore. In absence of temperature logs, only shutting off the open hole in the permeable Mississippian and within the directly connected highly fractured top of the Precambrian would yield an indication for the temperature at depth, if the well would still flow under such conditions.

The producible fraction of the reservoir's thermal energy is described by using a thermal recovery factor (Nathenson, 1975). The challenge in this resource assessment lies in quantifying the size and thermal energy of our reservoir as well as the constraints on extracting that thermal energy. It is possible to produce many times the original volume of fluid from the reservoir in order to recover all the thermal energy from the encompassing reservoir rock. The hot reservoir fluid is gradually replaced by colder water through natural recharge or by injection during power production. The recovery factor can easily range from 5 to 20 %, leaving a large uncertainty regarding potential geothermal power production (Lovekin, 2004).

Table 1 shows single well power production models based upon productivity index, production rate and fluid temperature. Those calculations by Albrecht are based on Sanyal et al. (2005) and Sanyal et al. (2007) but with proprietary computations of utilization efficiencies that are based upon power generation system design and a more accurate determination of enthalpy and thermal efficiencies resulting in very conservative estimates. The thermal recovery factor is a function of all those parameters.

Table 1: Single well power production modeling

Productivity Index (gpm/psi)	Production Rate (gpm)	Fluid Temperature (°F)	Net Power (MWe)
5	2450	200	1.6
5	2450	250	3.3
5	2450	300	5.3
6	2936	200	1.9
6	2936	250	3.9
6	2936	300	6.3

The single well power production model clearly demonstrates the influence of temperature variations on the overall reservoir power generation potential. The model also shows how sensitive the power generation potential is with respect to the measured flow at available pressure drawdown. This reflects reservoir permeability and available fluid volume, and how the increase of available flow gains importance as fluid temperature is increased.

Given the uncertainties at this time in quantifying the volume of the geothermal reservoir and its temperature, as well as the recovery factor in general, Monte Carlo simulation can only provide limited comfort in estimating the power generation potential of the complete geothermal reservoir at the project site. Simulation results of 10 MWe electric power generation potential appear feasible. A more reliable estimate will be available after the first well has been drilled.

3. Drilling

3.1 Drilling Objectives

The main objectives for the planning and design of the first exploration well were as follows:

- Verification of the seismic data and the results of the innovative elastic wave processing (amended fault traces). As the extension and strike direction of the Indian Springs fault zone to the South is uncertain and due to the objectives requested (verification of the MT „cup“ structure, hydrothermal feed in zones and the results of the innovative seismic elastic wave processing) the spud in into the drilling target area was determined as presented in Figure 14.
- Verification of the Permian rocks for geothermal utilization.
- Determination of the depth of the Precambrian rocks and verification if a weathered zone can be utilized as a reservoir. Determination of the depth of the sound Precambrian rock.
- Determination of the productivity of the expected reservoir drilling almost perpendicular into the dipping planes of the Indian Spring fault system.
- Verification of the origin of the „cup“ structure as surveyed through Magneto-Telluric.

Due to surface constraints, such as archaeological sites and a planned highway, the spud-in of the well was placed as shown in Figure 15.

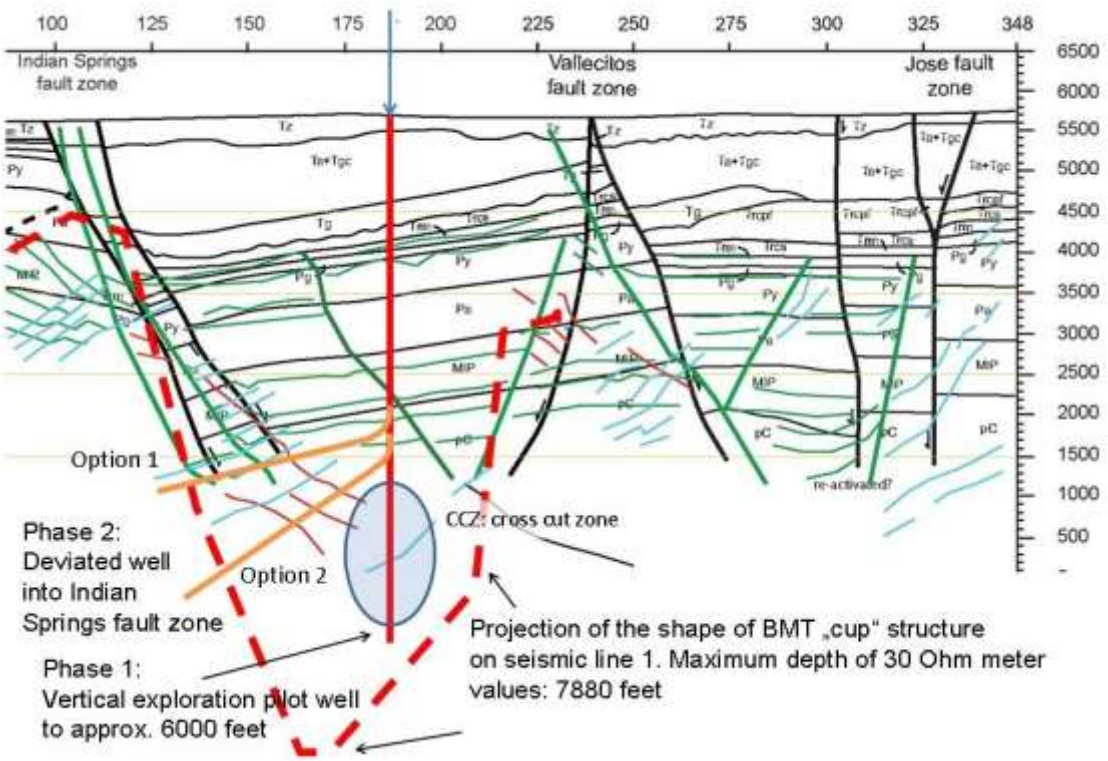

Figure 14: Schematic drilling options to explore the drilling objectives.

Figure 15: Spud-in point at the drilling target area: N 35° 35´04.10"; W 106° 44`1.73". The location is east of Highway 4, north-east of San Ysidro.

3.2 Drilling Operation

After building 1,000 yards of access road, a drill pad, and three drill pits, drilling started on October 17, 2013 (see Figure 16), and finished November 23, 2013 with an airlift (see Figure 17) after reaching a total depth of 5,657 feet. The well has a 68# J55 13 3/8" surface casing down to 4,136 feet and a 12 ¼" open hole to total depth. The 13 3/8" surface casing is placed in 626 feet of 18 5/8" casing. The spud in has been configured with a 30" conductor of 80 feet.

Figure 16: Jemez-GT-01 drill site on October 17, 2013.

As a sovereign nation, the Pueblo of Jemez is not regulated by State drilling regulations. Yet, without waiving its sovereign rights, the Pueblo agreed to follow the regulations of the State of New Mexico and utilize a vendor regulator for compliance management.

Figure 17: Jemez-GT-01 airlift on November 23, 2013.

The drill rig used was a 2005 Heartland HRI-700 with a Hacker 22” 0-150 rpm rotary drive. The derrick had a weight capacity of 365,000 lbs. During the complete drilling operation no problems with controlling water flow or with lost circulation were reported. 9.0 to 9.1 ppg mud weight were used during the drilling of the 12 ¼” section of the hole. That mud weight can be considered normal. It is possible that the drilling time did a good cooling of the rocks and after the well has been airlifted the well wanted to flow but there was not enough time available to heat it up. Chapter 4.3 describes the only problem that had to be negotiated during drilling; an extreme reduction of rate of penetration. The drilling operation was able to identify all structural elements, confirm the geological model, as identified prior through the surface geophysical methods. All hydrogeological questions require additional well logging and well testing.

3.3 Drill Path

Following the drilling objectives as outlined in Chapter 3.1 as well as the need for budget control, site geophysicist and Technical Project Manager Michael Albrecht geosteered the drilling operation 24/7 to reach the geological targets and reach them within budget, based upon the geological information, drilling performance parameters and operational cost factors, gathered while drilling. All structures and significant lithological changes were encountered where anticipated, given an additional dip towards south of about five degrees compared to the cross section as shown in Figure 13. Lithological changes within the first 3,300 feet were not as clear as anticipated by the project geologists.

Figure 18 shows the result of the deviation surveys.

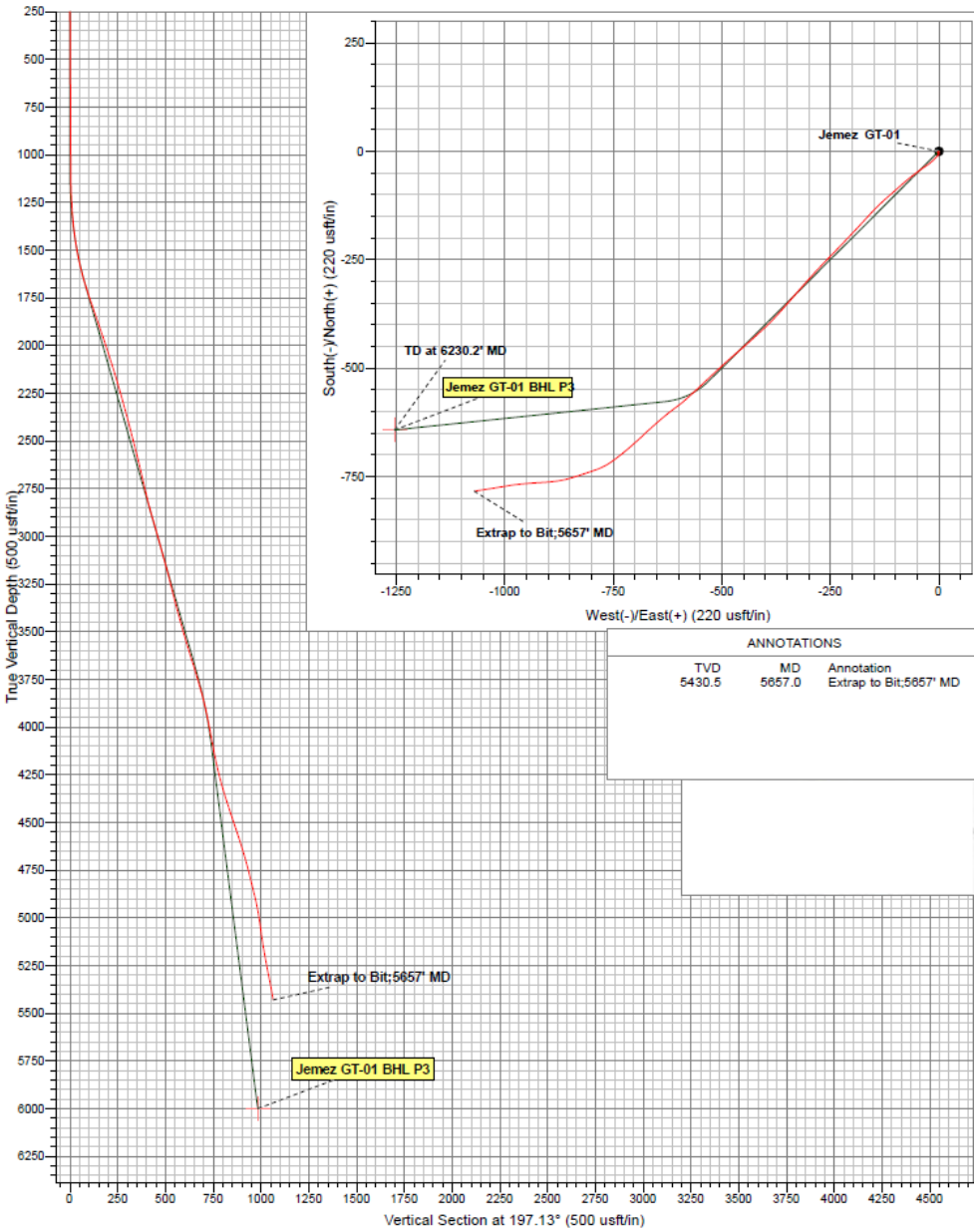

Figure 18: Final deviation survey of Jemez-GT-01.

Figure 19 shows how the drill path intersects the faults in Precambrian and the cup itself. Note that the 3-D rendering of the 2-D BMT profiles is based on Figure 8 (a) inversion and not Figure 8 (b) inversion. It was found to be more accurate to include BMT station k09 in the inversion of Profile J. According to Figure 8 (b), Figure 19 with k09 included in the inversion of Profile J would show that the well has been steered directly into target.

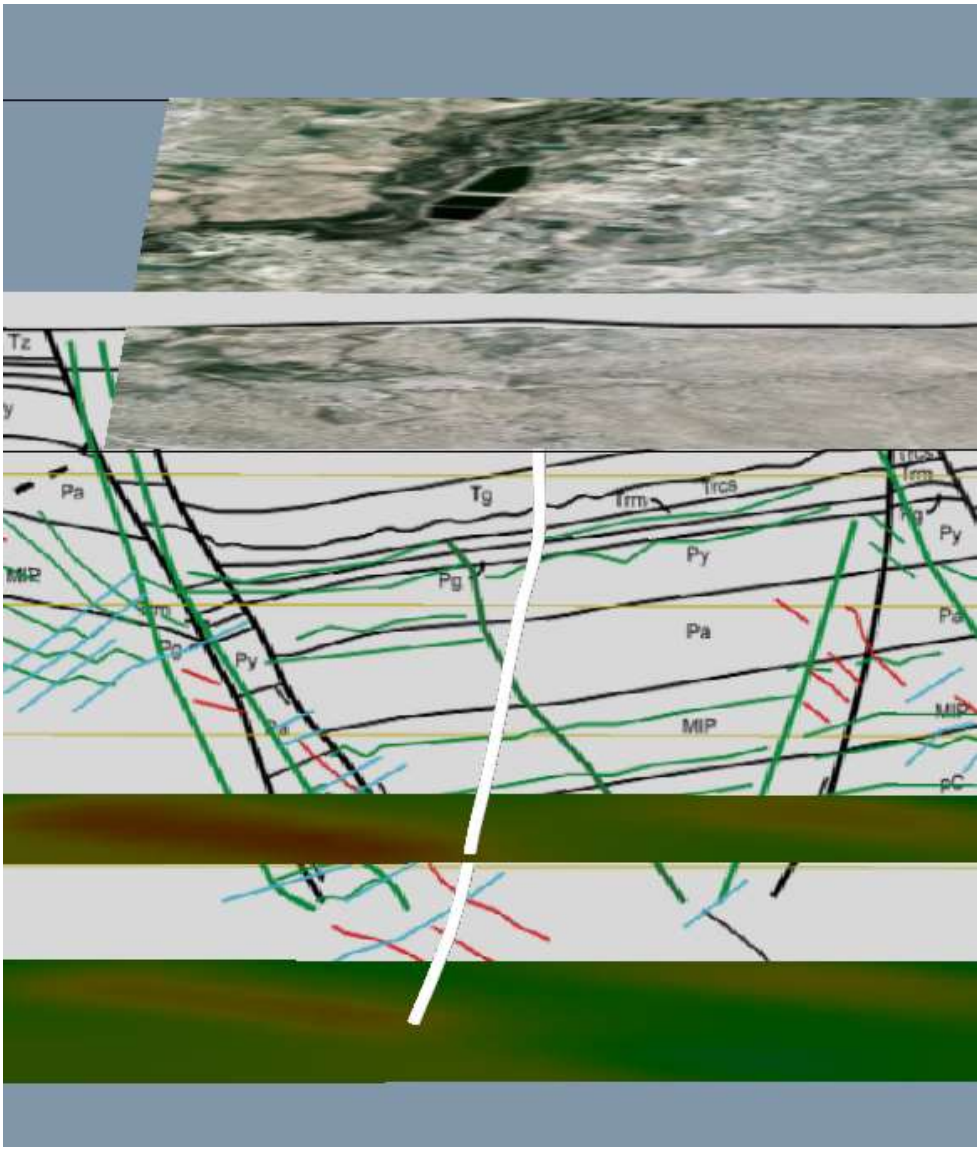

Figure 19: 3-D visualization of the drill path along a 3D MT rendering without k09. The top Magneto-Telluric plane crosses the well at 4,136 feet, the depth of the casing shoe. The bottom Magneto-Telluric plane crosses the well at total depth. Given Figure 8, the well clearly intersected with the “cup”.

4 Geological Findings

4.1 Rock Units

The following rock units have been encountered during drilling operations:

Rock Unit	*Depth Interval (feet)*		*Description*
Miocene Zia Sandstone	0	620	The Zia Sandstone is primarily tan, fine- to medium-grained, moderately-sorted sandstone composed of subround to well-rounded to angular grains of quartz and minor feldspar and magnetite. Lithic grains make up 1 to 5% of the sandstone and are commonly coarse-grained sand to granules in size. Lithic fragments include black, red, brown, white or yellow quartzite, porphyritic pink volcanic rock with phenocrysts of plagioclase and pyroxene (5-15% of the volcanic rock), white aphyric pumice, and a few Proterozoic metamorphic rocks (amphibolite, schist). The sandstone is generally weakly cemented, but the unit can be locally well-cemented in the vicinity of faults. Cementation was noted at 240 to 250 ft.
Oligocene Abiquiu Formation	620	1380	The sandstone composition of the light brown Abiquiu Formation is virtually identical to that of the Zia Sandstone, but the Abiquiu Formation contains a few granules of crystal-rich (35% phenocrysts) porphyritic volcanic rock with phenocrysts of plagioclase and pyroxene and a trace of Proterozoic granite. The Abiquiu is distinguished from the Zia Sandstone by the presence of very fine-grained ash with tiny grains of biotite and amphibole. The unit is variably moderately to weakly cement; similar to observations in outcrop.
Triassic Salitral Shale Member of the Chinle Group	1380	1460	The Salitral Shale is a red mudstone to siltstone with lenses of massive to crystalline calcite. The Salitral Shale is unconformably overlain by the Abiquiu Formation.

Triassic Agua Zarca Member of the Chinle Group	1460	1870	The upper part of this member is well-cemented quartz sandstone with well-rounded to angular, well-sorted, fine- to coarse-grained sand. Limonite and goethite staining of the sand grains is common. Trace amounts of muscovite are present. The lower part of this member is conglomeratic sandstone with lenses of white, brown, and black chert pebbles and petrified wood.
Fault zone within the Agua Zarca Formation	1740	1830	White, chalky vein fill within the sandstone is fractured and filled with silica.
Triassic Moenkopi Formation	1870	1890	Red siltstone with a trace of limestone.
Permian Glorieta Sandstone	1890	1980	The white to yellowish white Glorieta Sandstone is composed mainly medium-grained, well-sorted, round to subround to subangular, frosted quartz sand. White cement between sand grains does not react to acid, indicating silica cement. A trace of muscovite occurs in this unit. The gradational lower contact of the Glorieta Sandstone with the underlying Yeso Formation contains alternating red and white sandstone beds. The red sandstone has contains sand-sized quartzite that is red, yellow, and gray in color.
Permian San Ysidro Member of the Yeso Formation	1980	2380	The member is generally made up of loose sand grains near the top. Most of the interval is red, medium- to fine- to very fine-grained, well-cemented sandstone with well-rounded to angular, moderately-sorted quartz sand. Biotite is present in the very fine-grained sandstone near the base of the unit. Red to gray siltstone is present between 2080 and 2090 feet. Thin dolomite beds are at 2090 to 2110 feet and 2130 to 2150 feet; the dolomite contains a few fractures. A quartz vein cuts the sandstone at 2200 to 2210 feet.
Permian Meseta Blanca Member of the Yeso Formation	2380	2600	Orange-red sandstone with round to subround, medium- to coarse-grained sand grains; a few of the quartz and potassium feldspar grains are angular. The sandstone is finer-grained and the grains are more angular near the base of the unit.

Permian Abo Formation	2600	3520	The Abo Formation is composed of primarily of red siltstone, although green siltstone is also present. Sandstone intervals are red to white with very fine to medium to coarse, angular grains of quartz, potassium feldspar, muscovite, and biotite; the sandstone is cemented with carbonate. Conglomeratic intervals contain chert and quartzite pebbles. Thin beds of pedogenic carbonate occur throughout the unit. Localized redbed copper mineralization is found near the base of the Abo Formation.
Transitional Abo Formation and Madera Limestone	3520	3770	Micrite and silty limestone are interbedded with red to gray siltstone and sandstone containing grains of biotite and muscovite. Fracturing and pyrite were observed in this interval.
Madera Limestone	3770	4050	Light gray, fossiliferous micrite is the dominant rock type; silty limestone is less common. Calcite filled fractures are present in this interval.
Sandia Formation	4050	?	White, very fine-grained to fine-grained sandstone with quartz and muscovite characterizes the Sandia Formation.
Mississippian	?	4280	The Mississippian in this interval consists of white fine-grained sandstone, micaceous shale, and siltstone with traces of Proterozoic amphibolite and granite. This interval is mineralized with a gray fibrous mineral that is replaced by pyrite.
Proterozoic granite	4280 4860	4740 4940	The granite is relatively fresh and is composed of potassium feldspar, quartz, biotite, muscovite, and magnetite. Trace amounts of pyrite and chlorite are present.
Proterozoic porphyritic granite	4740	4860	This intrusion (dike or sill) has a gray aphanitic matrix and phenocrysts of potassium feldspar, quartz, and biotite.
Fault zone	4940	5300	The rock in the fault zone is Proterozoic granite, but the biotite is altered to chlorite and the pink feldspar is altered to clay or is altered to a tan color.
Proterozoic granite	5300	5460	The granite is relatively fresh and is composed of potassium feldspar, quartz, biotite, muscovite, and magnetite. Trace amounts of pyrite and chlorite are present.
Titanite granite	5460	5660	Similar to the Proterozoic granite by contains ~1% brown titanite.

There appears to be a fault zone in the granite between 4,940 feet and 5,300 feet where the biotite is altered to chlorite. The temperature of formation of chlorite seems to vary widely from 100 to 300°C. At this point in time it is not clear if the chlorite might in fact be a smectite (low temperature) or illit/smectite if altercation was at high temperature.

This work presented is preliminary and should be continued. It appears to be appropriate to document lithologic transitions and petrographic descriptions here to allow for continued discussion. Appendix E shows the complete mud log of the drilling operation as supporting document.

4.2 Lithologic Transitions

The drilling cuttings from 130' to 3045' have been analyzed using a binocular microscope. Several color and/or lithologic (rock type) transitions were noted during the examination. The transitions are located at the following *depths:*

Depth (feet)	*Transition*
630-640	Cuttings look like Zia Formation sands with rounded white pumices plus gray silty sandstone fragments (5-10%)
1000-1025	Medium gray sandstone/siltstone fragments that are different from the grayish sandstone (possibly Abiquiu Sandstone)
1100-1105	Brownish gray sands with few gray sandstone/siltstone fragments and rounded pumice
1420-1430	Reddish brown claystone with fine-grained clasts (possibly gypsum or anhydrite)
1480-1490	Agua Zarca sandstone
1820-1830	Abundant pinkish or reddish gray sandstone fragments and minor white quartz grains
1890-1900	White, well-sorted sand with few stained grains
1930-1940	Reddish gray stained sands and dark gray fragments
2020-2030	Reddish gray sands with medium gray opal fragments
2090-2100	Reddish gray sandstone with medium gray limestone fragments (30%)
2260-2270	Reddish gray sands and sandstone fragments with abundant medium gray opal fragments
2610-2620	Reddish gray sandstone and sands with abundant medium gray opal fragments
2910-2920	Grayish red sands and abundant medium gray opal fragments

3000-3005	Grayish red sandstone and sands, medium gray opal (10%) plus some reddish brown siltstone/claystone with abundant mica and few fine-grained white fragments that react with dilute acid.
3040-3045	Mixture of reddish brown siltstone/claystone with abundant mica, reddish gray sandstone fragments, and medium gray opal fragments, abundant clear quartz aggregates, and few fine-grained white clasts that react with dilute acid.

Most of the transitions clearly correlate with the porosity and caliber logs. At about 400 feet, the fragments contain a white matrix and at 650 feet, the amount of gray siltstone increases. It might be a transition from the Zia Formation to Abiquiu. Similar transitions are noted at about 1000 feet, 1100 feet. The transition to Agua Zarca is clearly marked at 1480-1490 feet. Thus there is a good correlation between the lithologic changes and porosity.

4.3 Petrographic Descriptions

Based upon on analysis of the cuttings obtained during mud logging a petrographic description has been identified as follows:

Depth Range (feet)	*Description*
130-140	Sand - Minerals and rock fragments are subrounded to rounded. Sample consists of abundant quartz grains with subordinate feldspars and rock fragments. Quartz grains show widespread overgrowth while feldspars are partially to totally altered. Rock fragments are also partially altered and recrystallized. Rock fragments consist of volcanic, igneous, and sandstone types.
540-550	Sand – Same as previous sample but more rock fragments and partially altered feldspars noted. Quartz grains appear less abundant and most feldspars are fractured, angular to subangular. Most volcanic fragments are altered.
620-630	Sand – More or less similar to Sample 540-550.
1110-1120	Sand and sandstone fragments – Fine grained containing abundant altered rock fragments. Feldspar grains with microcline twinning are partially to totally altered. Overgrowth commonly noted on subrounded to rounded quartz minerals. Sandstone fragments with clayey matrix are recrystallized.
1400-1420	Silty clay – Sample contains abundant fine-grained quartz and feldspar in a reddish brown clay matrix. Quartz and feldspar grains are subangular to subrounded. Feldspars are partially altered and a few calcite fragments were noted.

1480-1490	Sandstone – Fine grained, mostly clast supported and moderately sorted. Quartz and feldspar grains are subangular to subrounded and large siltstone clasts that are partially deformed with oriented grains are present. Siltstone clasts are generally recrystallized.
1780-1800	Sand and sandstone fragments – Sample consist of abundant coarse quartz and feldspar grains with minor recrystallized clast-supported sandstone plus a few siltstone and silty clay clasts. Larger feldspar grains are totally altered. Some large clay clasts contain microcrystalline quartz along fractures. Large isotropic (black) fragments (claystone?) that wrap around quartz grains were also noted.
1960-1980	Sand- Abundant subrounded to rounded quartz grains with overgrowth and minor feldspar and recrystallized rock fragments noted.
2020-2030	Sand – Sample contains abundant quartz with minor overgrowth and feldspar and minor rock fragments of recrystallized siltstone, and calcite-cemented sandstone. Quartz and mostly fractured feldspars are subangular to subrounded. Some rock fragments are fine grained and totally altered.
2320-2330	Sandstone – Contains abundant subrounded to rounded quartz and feldspar grains. Feldspars with common microcline twinning are fractured and partially altered. Overgrowth noted in quartz grains. Matrix-supported reddish brown siltstone fragments with comparable amounts of feldspar and quartz grain and a few large carbonate fragments were noted.
2420-2440	Sands and siltstone – Reddish siltstone contains comparable amounts of subangular to subrounded quartz and partially altered feldspars in a clayey matrix. Minerals have light reddish coating. Feldspars exhibit microcline twinning, whereas quartz grains show shadowy extinction. Some siltstone fragments are cemented with calcite.
2680-2690	Siltstone – Rock fragments are reddish brown. Siltstone fragments are calcite-cemented, whereas others are silica cemented and recrystallized. Sample contains a few coarse quartz and feldspar grains.
3470-3480	Mixed rock fragments – sample contains sandstone, siltstone, and claystone fragments. Both sandstone and siltstone fragments contain clayey matrix. Fine-grained carbonate fragments were also noted.
3810-3820	Carbonate – Recrystallized carbonate fragments with fossil pseduomorphs. Few silty clay fragments present.
4030-4040	Carbonate – Mostly recrystallized carbonate fragments with minor quartz, feldspar and silty clay contaminants.
4270-4280	Rock fragments - Mixture of recrystallized siltstone, sandstone, and carbonate fragments. Recrystallized sandstone fragments are clast-supported, carbonate-

	cemented, and appear partially deformed. Some large feldspar grains are altered and replaced by calcite. Quartz grains also exhibit considerable overgrowth. Minor muscovite grains noted.
4280-4300	Granite – Mixture of abundant quartz, feldspar, muscovite, pyrite, hornblende, and carbonate fragments. Minerals are mostly coarse grained, angular, and fractured. Feldspars are partially altered and quartz grains are slightly deformed and exhibit shadowy extinction.
4320-4340	Granite – Mixture of poorly sorted mineral assemblage of quartz, muscovite, feldspar, and few rock fragments. Feldspars are fractured and partially altered. Large clasts are totally replaced with calcite.
4560-4580	Granite – Sample consist of large, coarse-grained, angular quartz and feldspar grains and few biotite. Feldspars are fractured, partially altered, and exhibit microcline twinning. Some feldspar grains are replaced by calcite.
4970-4980	Granite – Sample contains a mixture of angular and fractured quartz, feldspar and partially deformed biotite.
5640-5650	Granite – Mixture of coarse and fractured quartz with significant overgrowth. Feldspar grains are also fractured and partially altered. Coarse biotite grains are deformed. Few hornblende crystals were also noted.

4.4 Wireline and Rig Data Logging

Funding for the final geophysical wireline logging has been made available only more than 6 months after drilling was completed. Subsequently, during the logging in summer 2014, the wireline tool encountered an obstruction in the well that couldn't be passed at about 4,180 feet depth. Through funding from another project a bailer has been utilized in an attempt to remove the obstruction. That attempt was not successful due to the amount of particles on the down facing side of the inclined well. The Pueblo of Jemez is expecting funding for a clean out operation with a regular drill rig in order to continue with the geophysical wireline logging and conduct hydrogeological well testing. Figure 20 shows the whiteboard of different Jemez-GT-01 logs (wireline and drill rig parameters).

The logged temperature in Figure 20 shows a negative temperature gradient starting at about 3,300 feet. That depth appears to be correlating with the discontinuity imaged by the elastic-wave reverse-time migration with a wavefield-separation imaging condition. That discontinuity (colored in green) does not reach the surface and the well path intersected it at around seismic station 175 and a depth of 3,300 feet. The change of the temperature gradient is very gradual. That correlates with the observations made during drilling; the rate of penetration (ROP) slowed down extremely when crossing that area and the drill bit was not steerable. Drilling nearly came to a standstill. Yet, cuttings and mineralogical analysis have shown no alterations of any kind, or changes in lithology. At this point in time, it has to be assumed that the discontinuity is structural, and not another fault. That discontinuity appears to limit the "cup" towards east.

The drill rig parameters (WOB, MSE, and ROP) reveal that the well intersected as expected several well defined fractures in granite after passing through a highly permeable zone within the Mississippian and top Precambrian. The well-defined fractures correlate with the faults marked in red in Figure 19. The well is currently artesian at a flow rate of 20 gpm with a well head pressure of 50 psi. Due to the analysis of the artesian water, it is currently assumed that it originates from a surface recharge penetrating through the highly permeable Mississippian with a well head temperature of about 155 Fahrenheit at a maximum equilibrium at depth between 158 Fahrenheit and 230 Fahrenheit (see Chapter 1.2). The well head pressure did not change over time, even after bailing operations confirmed an obstruction at about 4,180 feet, what would exclude the possibility of artesian flow of fluids from below 4,180 feet. Consequently, the flow currently encountered at the well head is not the deep fluid representing the main drilling target. Because the well is not cased in the permeable Mississippian, the pressure the fluid is under causes it to rise in the wellbore. In absence of temperature logs, only casing the open hole in the permeable Mississippian and within the directly connected highly fractured top of the Precambrian would yield an indication for the temperature at total depth, if the well would still flow under such conditions. For geothermal power production the depth between 4,180 feet and 5,657 feet needs to be analyzed. To date the temperature profile and hydrogeochemistry below about 4,150 feet are unknown. Also, Jemez-GT-01 is an exploration well. It is not a finished production well. The well has been designed in a way that it allows to be deepened to about 8,000 feet if necessary, following the results of a complete logging and well testing. Consequently, once determined, the temperature gradient below Mississippian ought to be projected to that depth.

The gradient starting at around 3,300 feet might as well be negative because drilling entered the cooler side of the convection cell. That would mean that the convection as outlined in Figure 11 is limited to the area between the Indian Springs Fault Zone and the discontinuity that does not reach the surface and is connected to the cross cut zone as shown in Figure 14. Further logging, water sampling at the bottom of the well, and hydrological well testing are necessary to better support the related discussion and avoid speculations.

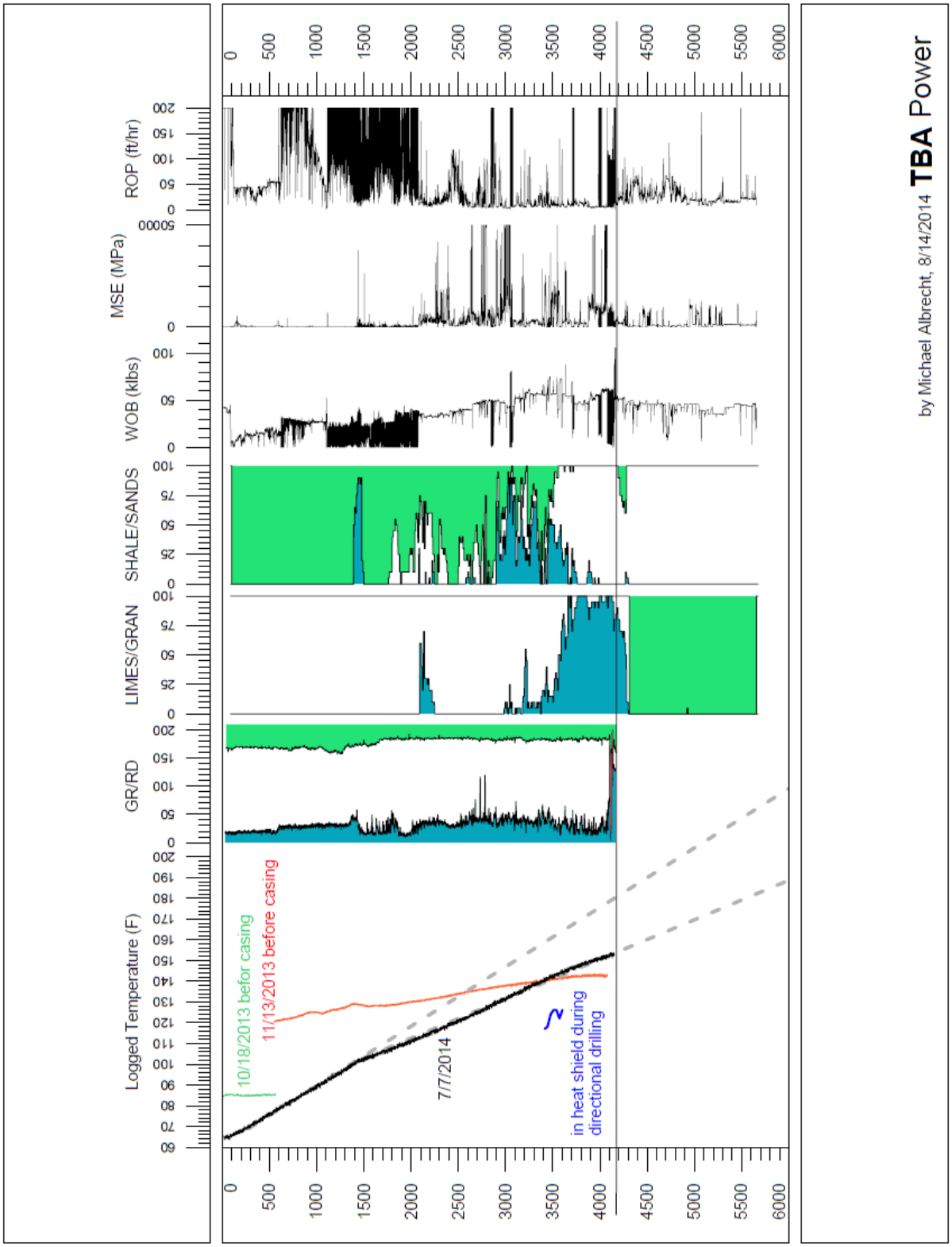

Figure 20: Whiteboard of wireline and rig data logs from Jemez-GT-01

5. Conclusions

The original assumption at the beginning of this project was that the first well will be drilled west of the Indian Springs Fault zone. Due to the multi-disciplined approach of the project a very detailed conceptual model of the study area has been developed and the original drilling assumption has been adjusted to east of the Indian Springs Fault Zone.

Even though it appears as if seismic as survey method is currently not very popular in the United States, the work in this project clearly shows how high resolution seismic can be conducted at a very reasonable price and how valuable the structural knowledge is obtained out of such survey. **Seismic studies conducted at other sites differ from the one conducted at Jemez Pueblo in geophone spacing, the type of source used, static array versus roll along, the use of very experienced professional processing providers versus the use of much less experienced university and National Laboratory personnel.** Certainly interbedded volcanic units might affect the results of a seismic survey but in large their existence alone cannot justify issues with seismic data interpretation in general.

Compared to vibroseis and explosives, the seismic source chosen for this project, an accelerated weight-drop system, has proven to be extremely more cost effective and significantly superior in regards to performance (energy coupling and frequency range). Traditional seismic processing (Kirchhoff or Wave-Equation Migration) delivers excellent results when processing data collected in a high resolution static array survey that covers the entire seismic line. Additional innovative processing clearly exceeded the expectations even of those who performed the processing.

Drilling confirmed all structural elements and conductivity differences as determined by the geophysical surface surveys. Magneto-Telluric alone would not have been able to provide responsibly drillable structural information. The combination of structural information obtained through seismic and conductivity information obtained by Magneto-Telluric resulted in a solid conceptual model of the resource. Each survey method alone would not have been able to provide a comparable resource model.

Low Frequency Magneto-Telluric (LMT) shows an area different from the chosen drilling target area that has enormous geothermal potential. Yet, due to a depth of about 12,000 feet, what is a reflection of the frequency range that detected it, that area can only be targeted in a separate project with a significant higher budget. As a consequence it is important to note that **not utilizing LMT data acquisition in addition to Broadband Frequency Magneto-Telluric (BMT) can result in deeper resources remaining undetected**.

The geosteering during the drilling operation was very successfully guided by the profiles shown in Figure 13 and Figure 14.

Until the geophysical logging and hydrogeological testing of the well are completed, no assessments can be made in regards to the geothermal potential of the well. All geochemical and temperature information obtained to date is limited to 4,180 feet and does not reflect the drilling target, what was the deeper "cup".

The well as drilled is suitable for direct use (see Chapter 1.2) and as drinking water supply to the Pueblo of Jemez. This means that the project already met its stated goal. An assessment in regards to its use for geothermal power production is pending further testing and investigation.

6. References

Formento-Trijilio, M. L., and Pazzaglia, F. J., 1998, Tectonic geomorphology of Sierra Nacimiento: Traditional and new techniques in assessing long-term landscape evolution of the southern Rocky Mountains: Journal of Geology, v. 106, p. 433–453.

Goff, F., and Shevenell, L., 1987, Travertine deposits at Soda Dam, New Mexico and their implications for the age and evolution of the Valles Caldera hydrothermal system: Bulletin of the Geological Society of America, v. 99, p. 292-302.

Goff, F., Shevenell, L., Gardner, J., Vuataz, F., and Grigsby, C., 1988. The hydrothermal outflow plume of Valles caldera, New Mexico and a comparison with other outflow plumes. Journal of Geophysical Research, v. 93(B6), p. 6041-6058.

Goff, F., Gardner, J.N., Reneau, S.L., and Goff, C.J., 2005, Preliminary geologic map of the Redondo Peak quadrangle, Sandoval County, New Mexico. NM Bureau Geology & Mineral Resources, Open-file Geologic Map OF-GM-111, scale 1:24,000.

Harrison, T.M., Morgan, P., Blackwell, D.D., 1986, Constraints on the age of heating at the Fenton Hill Site, Valles Caldera, New Mexico. Journal of Geophysical Research, Volume 91, Issue B2.

Huang L., Zhang Z., Rehfeldt K., Kelley S., Albrecht M., Kaufman G., 2011, Imaging Faults with Reverse-Time Migration for Geothermal Exploration at Jemez Pueblo in New Mexico, Proceedings, Geothermal Research Council Annual Meeting, San Diego, California, 2011.

Kelley, V.C., 1977, Geology of the Albuquerque basin, New Mexico: New Mexico Bureau of Mines and Mineral Resources Memoir 33, 59 p.

Kelley, S.A., Kempter, K.A., Goff, F., Rampey, M., Osburn, G.R., and Ferguson, C.A., 2003, Geology of the Jemez Springs 7.5 minute quadrangle, Sandoval County, New Mexico, New Mexico Bureau of Geology and Mineral Resources Open-file Geologic Map OF-GM73, scale 1:24,000.

Lovekin, J., 2004, Geothermal inventory: Bulletin, Geothermal Resources Council, v. 33, no. 6, p. 242-244.

Nathenson, M., 1975, Physical factors determining the fraction of stored energy recoverable from hydrothermal convection systems and conduction-dominated areas: U.S. Geological Survey, Open-File Report 75-525.

Osburn, G.R., Kelley, S., Rampey, M., and Ferguson, C.A., 2002, Geology of the Ponderosa 7.5-min. quadrangle, Sandoval County, New Mexico, New Mexico Bureau of Geology and Mineral Resources Open-file Geologic Map OF-GM57a, scale 1:24,000.

Pazzaglia, F. J.; Pederson, J. L.; Garcia, A. F.; Koning, D. J.; Formento-Trigilio, M.L.; Toya, C., 1998, Geology of the Jemez Pueblo 7.5-minute quadrangle: New Mexico Bureau of Geology and Mineral Resources Open-file Geologic Map OF-GM14. scale 1:24000.

Sanyal, S., Kitz, K., and Glaspey, D., 2005, Optimization of Power Generation from Moderate Temperature Geothermal Systems – A Case History, Proceedings World Geothermal Congress.

Sanyal, S., Morrow, J., and Butler, S., 2007, Net Power Capacity of Geothermal Wells Versus Reservoir Temperature – A Practical Perspective, Proceedings 32nd Stanford Workshop on Geothermal Reservoir Engineering.

Shevenell, L., Goff, F., Miles, D., Waibel, A., Swanberg, C., 1988, Lithologic Descriptions and Temperature Profiles of Five Wells in the Southwestern Valles Caldera Region, New Mexico, LA-11165-OBES, Los Alamos National Laboratory, NM.

Smith, R.L., Bailey, R.A., and Ross, C.S., 1970, Geologic map of the Jemez Mountains, New Mexico: United States Geological Survey Map I-571, scale 1:125,000.

Williams, C.F., Reed, M.J., and Mariner, R.H., 2008, A Review of methods applied by the U.S. Geological Survey in the assessment of identified geothermal resources, USGS Open-file report 2008-129.

Witcher, J.C., 2004, Pueblo of Jemez Geothermal Feasibility Project: Part 1 - Geotechnical Report, US DOE Contract DE-FC36-02GO12104.

WoldeGabriel, G., Kelley, S., 2011, Mineralogy, petrography, geochemistry, and U-series dating of travertine and sedimentary rocks from Pueblo of Jemez, New Mexico, LA-UR 11-00639, Los Alamos National Laboratory, NM.

Wood, G.H., Jr., and Northrop, S.A., 1946, Geology of the Nacimiento Mountains, San Pedro Mountain and adjacent plateaus in parts of Sandoval and Rio Arriba Counties, New Mexico: U.S. Geological Survey, Oil and Gas Investigations Preliminary Map 57.

Woodward, L.A., 1987, Geology and mineral resources of Sierra Nacimiento and vicinity, New Mexico: New Mexico Bureau of Mines and Mineral Resources, Memoir 42, 84 p.

Woodward, L.A. and Ruetschilling, R.L., 1976, Geology of the San Ysidro quadrangle, New Mexico: New Mexico Bureau of Mines and Mineral Resources, Geologic Map 37, scale 1:24,000.

Zonge International, Inc, 2011, Geophysical Investigation Report, 2D Seismic Reflection Survey Jemez Geothermal Project